Astrophysical Black Holes

Andrew C. Fabian and Anthony N. Lasenby

Abstract. Black holes are a common feature of the Universe. They are observed as stellar mass black holes spread throughout galaxies and as supermassive objects in their centres. Observations of stars orbiting close to the centre of our Galaxy provide detailed clear evidence for the presence of a 4 million Solar mass black hole. Gas accreting onto distant supermassive black holes produces the most luminous persistent sources of radiation observed, outshining galaxies as quasars. The energy generated by such displays may even profoundly affect the fate of a galaxy. We briefly review the history of black holes and relativistic astrophysics before exploring the observational evidence for black holes and reviewing current observations including black hole mass and spin. In parallel we outline the general relativistic derivation of the physical properties of black holes relevant to observation. Finally we speculate on future observations and touch on black hole thermodynamics and the extraction of energy from rotating black holes.

1 Introduction

Black holes are exotic relativistic objects which are common in the Universe. It has now been realised that they play a major role in the evolution of galaxies. Accretion of matter into them provides the power source for millions of high-energy sources spanning the entire electromagnetic spectrum. In this chapter we consider black holes from an astrophysical point of view, and highlight their astrophysical roles as well as providing details of the General Relativistic phenomena which are vital for their understanding.

To aid the reader in appreciating both aspects, we have provided two tracks through the material of this Chapter. Track 1 provides an overview of their astrophysical role and of their history within 20th and 21st century astrophysics. Track 2 (in italic text) provides the mathematical and physical details of what black holes are, and provides derivations of their properties within General Relativity. These two tracks are tied together in a way which we hope readers with a variety of astrophysical interests and persuasions will find useful.

2 A Brief History of Astrophysical Black Holes

Although the term "black hole" was coined by J.A. Wheeler in 1967, the concept of a black hole is over two hundred years old. In 1783, John Michell [41] was considering how to measure the mass of a star by the effect of its gravity on the speed of the light it emitted. Newton had earlier theorized that light consists of small particles. Michell realized that if a star had the same density as the Sun yet was 500 times larger in size, then light could not escape from it. The star would thus be invisible. He noted, however, that if it was orbited by a luminous star, the measurable motion of that star would betray the presence of the invisible one.

This prescient, but largely forgotten paper, embodies two important concepts. The first is that Newtonian light and gravity predicts a minimum radius $R = 2GM/c^2$ for a body of mass M from within which the body would not be visible. The second is that it can still be detected by its gravitational influence on neighbouring stars. The radius is now known as the Schwarzschild radius of General Relativity and is the radius of the event horizon of a non-spinning black hole. Black holes are now known to be common due to their gravitational effect on nearby stars and gas. Pursuing Newtonian black holes further leads to logical inconsistencies and also the problem that relativity requires the speed of light to be constant.

The concept re-emerged after the publication of Eintein's General Theory of Relativity in 1915 when Karl Schwarzschild found a solution for a point mass. Einstein himself "had not expected that the exact solution to the problem could be formulated". It was not realised at the time that the solution represented an object which would turn out to be common in the Universe. Chandrasekhar in 1931 [9] discovered an upper limit to the mass of a degenerate star and which implied the formation of black holes (although this was not spelled out). Eddington, who wrote the first book of General Relativity to appear in English, considered the inevitability of complete gravitational collapse to be a *reductio ad absurdum* of Chandrasekhar's formula. The concept was again ignored for a further two decades, apart from work by Oppenheimer and Snyder [50] who considered the collapse of a homogenous sphere of pressureless gas in GR, and found that the sphere becomes cut off from communication with the rest of the Universe. In fact, what they had discovered was the inevitability of the formation of a black hole when there is no pressure support.

With this brief introduction to the early history, we now give some details of what is now understood by a Schwarzschild black hole.

2.1 The Schwarzschild Metric

The simplest type of black hole is described by the Schwarzschild metric. This is a vacuum solution of the Einstein field equations in the static, spherically symmetric

case, and takes the form

$$ds^2 = \left(1 - \frac{2GM}{c^2 r}\right) dt^2 - \frac{1}{c^2}\left(1 - \frac{2GM}{c^2 r}\right)^{-1} dr^2 - \frac{r^2}{c^2} d\theta^2 - \frac{r^2 \sin^2 \theta}{c^2} d\phi^2 \quad (2.1)$$

where M is the mass of the central object. Most of the observational properties of black holes that we need follow from this metric, rather than needing the deeper level of the field equations themselves to understand them, but to give an indication of the achievement of Schwarzschild, and since we will wish to consider briefly more general spherically-symmetric black holes as well, we give a brief sketch of how the metric is derived. For more details, and a description of the sign conventions we are using, see Chapters 8 and 9 of [30].

The field equations themselves are

$$G_{\mu\nu} = -8\pi T_{\mu\nu} \quad (2.2)$$

where the Einstein *tensor $G_{\mu\nu}$ is a trace-reversed version of the* Ricci *tensor $R_{\mu\nu}$ and $T_{\mu\nu}$ is the matter stress-energy tensor (SET). If the matter SET is traceless, in particular if we are in a vacuum case, then clearly $G_{\mu\nu}$ must be traceless as well, and so the vacuum equations are that all components of the Ricci tensor are zero:*

$$R_{\mu\nu} = 0 \quad (2.3)$$

The Ricci tensor is in turn a contraction, $R_{\mu\nu} = R^{\lambda}{}_{\mu\nu\lambda}$ of the Riemann tensor, *which is defined by*

$$R^{\mu}{}_{\alpha\beta\gamma} = \frac{\partial \Gamma^{\mu}{}_{\alpha\gamma}}{\partial x^{\beta}} - \frac{\partial \Gamma^{\mu}{}_{\alpha\beta}}{\partial x^{\gamma}} + \Gamma^{\mu}{}_{\sigma\beta}\Gamma^{\sigma}{}_{\gamma\alpha} - \Gamma^{\mu}{}_{\sigma\gamma}\Gamma^{\sigma}{}_{\beta\alpha} \quad (2.4)$$

where $\Gamma^{\mu}{}_{\alpha\beta}$ is the connection. *For a general metric $g_{\mu\nu}$, defined by*

$$ds^2 = g_{\mu\nu} dx^{\mu} dx^{\nu} \quad (2.5)$$

the connection is given in terms of the metric by

$$\Gamma_{\mu\alpha\beta} = \frac{1}{2}\left(\frac{\partial g_{\mu\beta}}{\partial x^{\alpha}} + \frac{\partial g_{\alpha\mu}}{\partial x^{\beta}} - \frac{\partial g_{\alpha\beta}}{\partial x^{\mu}}\right) \quad (2.6)$$

We can thus see that solving the apparently simple equation (2.3) involves potentially formidably complicated second order partial differential equations, and it is not surprising that Einstein considered it unlikely that an exact solution for the metric around a spherical body would be found. In the current case, where we have assumed everything is static, we can attempt an ansatz for the metric which simplifies things considerably. We let

$$ds^2 = A\,dt^2 - B\,dr^2 - r^2\left(d\theta^2 + \sin^2\theta\,d\phi^2\right) \quad (2.7)$$

where A and B are functions of r alone. This means that our PDEs become ODEs, and although the working is still complicated, we eventually find that we require

$$R_{00} = -\frac{A''}{2B} + \frac{A'}{4B}\left(\frac{A'}{A} + \frac{B'}{B}\right) - \frac{A'}{rB} = 0, \tag{2.8}$$

$$R_{11} = \frac{A''}{2A} - \frac{A'}{4A}\left(\frac{A'}{A} + \frac{B'}{B}\right) - \frac{B'}{rB} = 0, \tag{2.9}$$

$$R_{22} = \frac{1}{B} - 1 + \frac{r}{2B}\left(\frac{A'}{A} - \frac{B'}{B}\right) = 0, \tag{2.10}$$

$$R_{33} = R_{22}\sin^2\theta = 0. \tag{2.11}$$

We can eliminate A and find a simple equation for B by forming the combination

$$\frac{R_{00}}{A} + \frac{R_{11}}{B} + \frac{2R_{22}}{r^2} = 0 \tag{2.12}$$

which yields the ODE

$$\frac{dB}{dr} = \frac{B(1-B)}{r} \tag{2.13}$$

with solution

$$B = \frac{r}{r+C} \tag{2.14}$$

where C is a constant. Inserting this in (2.10) then yields a first order equation for A of which the solution is

$$A = \frac{a(r+C)}{r} \tag{2.15}$$

where a is a further constant. This latter constant effectively just changes the units of time, and it is sensible to choose this so that the speed of light c is 1, which we temporarily employ. We have thereby recovered the Schwarzschild metric, (2.1), and can identify the constant C as $-2GM$.

One notices straightaway that some kind of singularity exists at $r = -C = 2GM$, but it is worth noting that this is not a singularity of the Riemann tensor (the only non-zero quantity transforming as a full tensor we have available for investigation). The entries of this all behave with r like $1/r^3$, corresponding to tidal forces which make neighbouring particles move apart or together in their motion, and none have a singularity at $r = 2GM$. Indeed, the form in which Schwarzschild first discovered his metric also had no singularity at this radius (see e.g. [63] and the comments in [1]), and this coupled with lack of singularity of the Riemann tensor except at the origin, perhaps contributed to the uncertainty stretching over many years as to the physical status of the distance $2GM$.

Nowadays, we of course recognise this as the "horizon", the point where light becomes trapped. We discuss this in more detail below, particularly in connection with

the Kerr solution, but we can understand this in simple terms by looking at the 'coordinate speed' of a light pulse. For such a pulse, the interval $ds = 0$, and for outward radial motion this means

$$Adt^2 - Bdr^2 = 0, \quad i.e. \quad \frac{dr}{dt} = \sqrt{\frac{A}{B}} \qquad (2.16)$$

The 'horizon' is therefore where the metric coefficient B goes to infinity, since this marks the point where light is no longer able to move outwards. This happens in the Schwarzschild case at $r = r_S = 2GM/c^2$, which is the location of the event horizon.

Before proceeding further, we mention a few physical facts about Schwarzschild black holes. The first is that the radius of the event horizon, r_S, corresponds to $3\,\mathrm{km}$ per Solar mass. This means that the mean density of a black hole is given by

$$\rho = 2 \times 10^{16} \left(\frac{M}{M_\odot} \right)^{-2} \mathrm{gm\,cc}^{-1}. \qquad (2.17)$$

Thus black holes with masses above $10^8 M_\odot$, have average densities below that of water, or the Sun. Those above a few billion $M_\odot$ have densities below that of air. So from a mean density point of view, supermassive black holes are not particularly dense. The light-crossing time of the event horizon (i.e. a length equivalent to its diameter) is $0.2\,ms$ for a $10 M_\odot$ black hole. $20\,s$ for $10^6 M_\odot$ and about one day for $5 \times 10^9 M_\odot$.

3 Relativistic Astrophysics emerges

The previous neglect of black holes changed in 1963 when two important events occurred, the discovery of quasars by Maarten Schmidt [61] and the discovery of the solution for a spinning black hole by Roy Kerr [31]. These combined to lead to Relativistic Astrophysics as the combination of Astrophysics and GR, embodied in the first Texas Symposium of Relativistic Astrophysics in December 1963. Kerr's brief talk has in retrospect been called the most important announcement at the Symposium but was not mentioned by any of the three summarizers of the meeting [62].

The discovery of quasars resulted from the accurate position for the cosmic radio source 3C273 obtained by Cyril Hazard and collaborators [29] using the lunar occultation technique. Schmidt used the 200" Hale Telescope to take an optical spectrum of the starlike object at that position in the Sky. Some weeks later he identified emission lines in the spectrum with Balmer lines of hydrogen, redshifted by 0.16. Interpreting the redshift as due to cosmic expansion means that it is at a (luminosity) distance of 0.75 Gpc. From its apparent brightness, the object can be inferred to be more than 10^{12} times more luminous than the Sun. 3C273 can be found on optical plates taken since the late 1800s and was soon shown to be variable, at times changing significantly within a week. Ignoring relativistic considerations, causality requires that significant variations cannot occur on timescales shorter than the light crossing time of the object.

It therefore appears that the prodigious power output of 3C273 emerges from a region of size similar to the Solar System! [1]
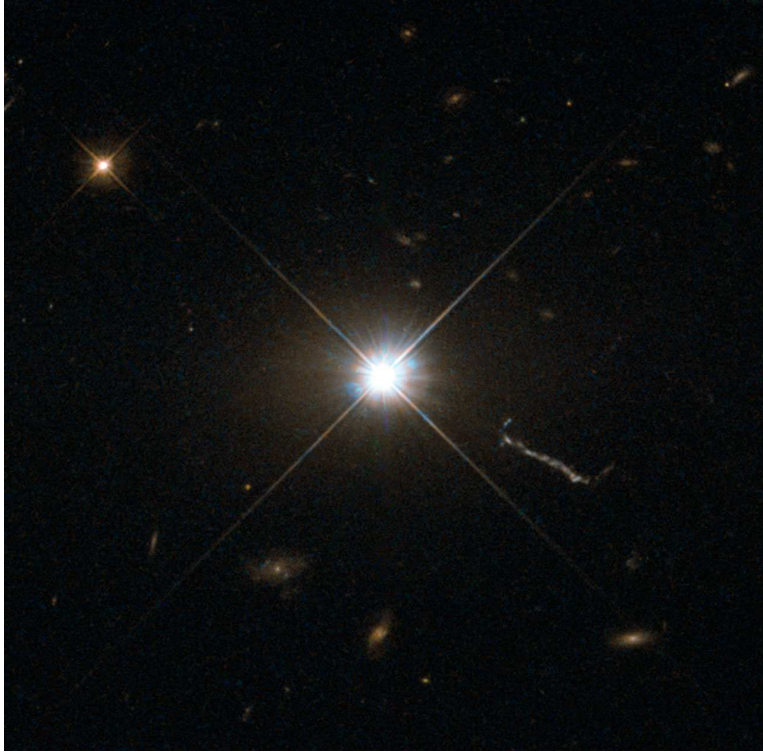
Figure 1. The first quasar identified, 3C273, as imaged by the Hubble Space Telescope. It lies over two billion light years away and is the brightest quasar in the visible Sky. The structure to the SW (lower right) is the outer parts of its relativistic jet, which is seen from radio to X-ray wavelengths. The projected length of the jet is over 200 thousand light years, so its true length is nearly an order of magnitude larger than our galaxy. The mass of its black hole has been measured by the optical reverberation technique at almost a billion Solar masses. The X-shape is an instrumental artefact created by support structures in the telescope; it implies that the source is unresolved. 3C273 varies on week-long timescales indicating that the emission region is less than a light week across.

Kerr's solution to the Einstein field equations was not immediately recognised as the exact solution for a spinning black hole. We now know the geometry described is the unique and complete description of the external gravitational field of an uncharged stationary black hole. It is now thought that the power of 3C273 and other quasars is due to accretion onto a Kerr black hole, which we now give some preliminary details

---

[1] 3C273 is not just a pointlike object but has an associated linear structure which we now know to be a relativistic jet, but the above argument is good for the main central source.

of.

3.1 Rotating black holes

It is now known that the totality of black holes can be described using just three parameters. Whatever makes them up, and however they were formed, in the end only three parameters matter — their mass, M; charge, Q and angular momentum J. Due to the high conductivity of interstellar matter, black holes are not likely to have a net charge for long, so the only relevant parameter in addition to mass is spin.[2] A metric applicable to a black hole with angular momentum was found by Kerr in 1962 [31]. This metric, in the form later developed by Boyer & Lindquist [6], is

$$
\begin{aligned}
ds^2 = \left(1 - \frac{2GMr}{\rho c^2}\right) dt^2 - \frac{1}{c^2} \left[\frac{-4GMra\sin^2\theta}{\rho c} dt d\phi + \frac{\rho}{\Delta} dr^2 \right. \\
\left. + \rho d\theta^2 + \left(r^2 + a^2 + \frac{2GMra^2\sin^2\theta}{\rho c^2}\right) \sin^2\theta d\phi^2 \right],
\end{aligned}
\tag{3.1}
$$

where $a = (J/Mc)$ is the angular momentum of the black hole per unit mass (and has the dimensions of distance), $\Delta = r^2 - (2GMr/c^2) + a^2$ and $\rho = r^2 + a^2\cos^2\theta$. Substituting this metric into equation (2.6) for the connection coefficients and calculating the Riemann (2.4) from these, the Ricci tensor $R_{\mu\nu} = R^\lambda{}_{\mu\nu\lambda}$ will be found to vanish, and therefore satisfy the vacuum field equations (2.3). This is a formidable calculation, however, and techniques which derive the metric in the context of more general azimuthally symmetric spacetimes (e.g. [14]) are in fact easier to carry out.

Note if the black hole is non-rotating, then $J = a = 0$ and the Kerr metric reduces to the standard Schwarzschild metric (2.1). Almost certainly, all real black holes in the universe will be of the Kerr type. The idea is that just as infalling matter will have angular momentum, so will the material from which the black hole formed, leaving it both with a mass and net angular momentum.

3.2 Black holes as energy sources

The enormous luminosity of 3C273 and other quasars was soon linked to black holes by Edwin Salpeter [60] and (separately) Yakov Zeldovich [78]. The energy is due to the deep gravitational potential well of the black hole which can be liberated by collisions outside the event horizon as gas falls in. If two gas clouds with small amounts of equal but opposite angular momenta fall into a Schwarzschild black hole colliding at $4r_g$ (note r_g is defined as GM/c^2) and momentarily coming to rest with their kinetic energy emitted as radiation, then about 29% of the rest mass energy of the clouds is

---

[2] Newman et al [48] found the solutions to the Einstein-Maxwell field equations in 1965 and the resulting Kerr-Newman geometry describes spinning charged black holes.

released. More generally the angular momentum will be much larger and the radiative efficiency of accretion smaller. A specific model involving an accretion disc was proposed by Donald Lynden-Bell [36] in 1969. Due to the small size of a black hole, it is most unlikely that gas falling into a black hole does so radially, but will have some angular momentum which will cause it to orbit the hole. Viscosity in the swirling gas will cause matter at smaller radii, which is moving faster, to transfer its angular momentum outward to material at larger radii, which is moving slower. The gas then spreads in radius forming an accretion disc in which angular momentum is transferred outward as matter flows inward. The accretion disc model of Lynden-Bell was then studied in a detail in the early 1970s by Pringle & Rees [58], Shakura & Sunyaev [65] and, for the Kerr metric, by Novikov & Thorne [49]. The gravitational energy liberated by the inflow heats the disc which radiates locally as a quasi-blackbody. The disc is thin but may extend outward for a considerable distance. This basic picture probably accounts for much of the energy liberated by accreting black holes. There are important modifications due to the magnetic nature of the ionized infalling plasma which will be discussed later. Accretion onto a black hole is the most mass-to-energy efficient process known, apart from direct matter-antimatter annihilation which, due to the rarity of antimatter in our universe, is highly uncommon. Such accretion may account for 20-30% of the energy released in the Universe since the recombination era. To understand the details of how this can happen, we now examine particle motion in GR, first generally, and then applied specifically to the question of efficiency of gravitational energy release around a Schwarzschild black hole. (The more complicated issue of energy release around a Kerr black hole is treated in Section 7.1.)

3.3 Motion in the Schwarzschild metric

The key to most astrophysical applications of the Schwarzschild metric is how point particles and photons move in it. In General Relativity, particles move on geodesics of the metric, i.e. the paths with an extremal lapse of proper time (for a massive particle) or 'affine parameter' (for a massless particle), along the worldline. If we let ds be the differential interval along a path, and s_{AB} the total interval between two points A and B on a given path, then with $\dot{x}_\mu \equiv dx_\mu/ds$ we have

$$s_{AB} = \int_A^B ds = \int_A^B [g_{\mu\nu} dx^\mu dx^\nu]^{\frac{1}{2}} = \int_A^B \left[g_{\mu\nu} \frac{dx^\mu}{ds} \frac{dx^\nu}{ds} \right]^{\frac{1}{2}} ds$$

$$= \int_A^B G(x^\mu, \dot{x}^\mu) \, ds \quad where \quad G(x^\mu, \dot{x}^\mu) = [g_{\mu\nu} \dot{x}^\mu \dot{x}^\nu]^{\frac{1}{2}}$$

(3.2)

and finding the path which extremises s_{AB} then leads to the Euler-Lagrange equations (one for each μ)

$$\frac{d}{ds} \left(\frac{\partial G}{\partial \dot{x}^\mu} \right) - \frac{\partial G}{\partial x^\mu} = 0$$

(3.3)

Note using the result (2.6) is is easy to demonstrate the equivalence of (3.3) with the alternative, and perhaps more familiar form

$$\frac{dx^\mu}{ds^2} + \Gamma^\mu{}_{\nu\sigma} \frac{dx^\nu}{ds} \frac{dx^\sigma}{ds} = 0 \tag{3.4}$$

The advantage of the former, (3.3), comes from the fact that it does not need knowledge of the connection coefficients to compute it, and also conservation laws for variables of which the metric is not an explicit function, are easy to read off. Note from its definition (compare the second and fifth quantities in the chain of equalities (3.2)), that as a numerical quantity $G(x^\mu, \dot{x}^\mu)$ evaluates to 1 (at least for a massive particle), which we can use to simplify formulae once its functional dependence has already been used.

So we now apply these results to the metric in the general static form given by (2.7). (The advantage of carrying this out for the general form, rather than just Schwarzschild, is that it enables us to consider results for other types of black hole, such as Reissner-Nordstrom, and Schwarzschild-de Sitter — see below.) We can assume w.l.o.g. that the particle motion is confined to the $\theta = \pi/2$ plane, and then the equations we find are

$$A\dot{t}^2 - B\dot{r}^2 - r^2\dot{\phi}^2 = 1 \tag{3.5}$$

coming from $G(x^\mu, \dot{x}^\mu) = 1$, and

$$A\dot{t} = k, \quad and \quad r^2\dot{\phi} = h \tag{3.6}$$

coming from the Euler-Lagrange equations in t and ϕ respectively, and where k and h are constants. These last two equations result from the constancy of the metric coefficients in t and ϕ and correspond to the conservation of energy and angular momentum. For a particle of mass m, kmc^2 can be identified as the particle energy, and h is the specific angular momentum per unit mass.

There is no point forming the Euler-Lagrange equation in r, since we already have a simple expression for $\dot{r}$ available from the combination of (3.5) and (3.6), yielding

$$\dot{r}^2 = \frac{1}{B}\left(\frac{k^2}{A} - \frac{h^2}{r^2} - 1\right) \tag{3.7}$$

We return to this general form later, but now wish to obtain results specific to the Schwarzschild case. With $A = B^{-1} = (1 - 2GM/r)$, and reinstating c for the remainder of this section, we obtain

$$\dot{r}^2 = c^2(k^2 - 1) - \frac{h^2}{r^2}\left(1 - \frac{2GM}{c^2 r}\right) + \frac{2GM}{r}. \tag{3.8}$$

Using the usual Newtonian substitution $u \equiv 1/r$, and changing the independent variable to azimuthal angle ϕ rather than the interval s, so that it is easier to discuss

the shape *of the orbit, we differentiate (3.8) to obtain*

$$\frac{d^2u}{d\phi^2} + u = \frac{GM}{h^2} + \frac{3GM}{c^2}u^2. \tag{3.9}$$

In Newtonian gravity, the equation for planetary orbits, in the same notation, is

$$\frac{d^2u}{d\phi^2} + u = \frac{GM}{h^2}, \tag{3.10}$$

so we have almost *got the Newtonian answer, except for the extra term* $3GMu^2/c^2$. *This is what gives all the relativistic effects, and we note it correctly goes to zero as* $c \to \infty$.

3.4   Circular orbits

An important application of the orbit formula in the context of high energy astrophysics, is what it tells us about circular *orbits in Schwarzschild geometry. These will be approximately the orbits of material* accreting *onto black holes, since infalling material nearly always has angular momentum, and we would not generally expect direct radial infall.*

If r *is constant, then our equation for* u *(3.9) yields*

$$h^2 = \frac{GMr^2}{r - 3GM/c^2}. \tag{3.11}$$

Putting $\dot{r} = 0$ *in equation (3.8) gives us*

$$\frac{h^2}{c^2r^2} = \frac{k^2r}{r - \frac{2GM}{c^2}} - 1 \tag{3.12}$$

and then putting both these last two results together yields an equation for k *in terms of* r *alone. We derive:*

$$k = \frac{1 - \frac{2GM}{rc^2}}{\sqrt{1 - \frac{3GM}{rc^2}}}. \tag{3.13}$$

Remembering $k = E/mc^2$, *where* E *is the particle energy, we have found that the energy of a particle in a circular orbit is*

$$E_{\text{circ}} = mc^2 \frac{1 - \frac{2GM}{rc^2}}{\sqrt{1 - \frac{3GM}{rc^2}}}. \tag{3.14}$$

An obvious check on this equation, is whether it can reproduce the Newtonian expression for the total energy of a circular orbit in the limit of large r. *Using the binomial theorem we see that indeed the first two terms in an asymptotic expansion in* r *are*

$$E_{\text{circ}} \sim mc^2 - \frac{GMm}{2r} + \dots, \tag{3.15}$$

Thus we get agreement at large r with the usual Newtonian expression (derived via

$$E_{\text{tot}} = K.E. + P.E. = \frac{1}{2}mv^2 - \frac{GMm}{r} = \frac{-GMm}{2r} \quad if \quad \frac{mv^2}{r} = \frac{GMm}{r^2}) \quad (3.16)$$

provided we realise that it enters as a correction *to the rest mass energy mc^2, which is the dominant term.*

The equation we have just found for the energy of a circular orbit, provides us with a remarkable amount of information about the nature of such orbits.

First we see that in the limit $m \to 0$, the orbit $r \to 3GM/c^2$ is of interest, since the singularity in the denominator can cancel the zero at the top. In fact this is the circular photon *orbit at $r = 3GM/c^2$, which we will derive below in a treatment of photon motion.*

Secondly, we can see which orbits (for particles of non-zero rest mass) are bound. *This will occur if $E_{\text{circ}} < mc^2$, since then we have less energy than the value for a stationary particle at inifinity. The condition for $E_{\text{circ}} = mc^2$ is that*

$$\left(1 - \frac{2GM}{rc^2}\right)^2 = 1 - \frac{3GM}{rc^2} \tag{3.17}$$

This happens for $r = 4GM/c^2$ or $r = \infty$. Thus over the range $4 < r < \infty$ the circular orbits are bound.

This appears to show we can get as close as 2 Schwarzschild radii to a black hole for particles in a circular orbit, suggesting that this is where the inner edge of any accretion disc would be. But is such an orbit stable*? We discuss this first in the specific context of the Schwarzschild metric, and then later look at stability in the context of more general metrics of the form (2.7).*

3.5 Stability of circular orbits

In Newtonian dynamics the equation of motion of a particle in a central potential is

$$\frac{1}{2}\left(\frac{dr}{dt}\right)^2 + V(r) = E, \tag{3.18}$$

where $V(r)$ is an "effective potential". For an orbit around a point mass, the effective potential is

$$V(r) = \frac{h^2}{2r^2} - \frac{GM}{r}, \tag{3.19}$$

where h is the specific angular momentum of the particle. Since the $1/r^2$ term will eventually always exceed the $1/r$ term as $r \to 0$, we can see that in Newtonian dynamics a non-zero angular momentum provides an angular momentum barrier *preventing a particle reaching $r = 0$ — see Fig. 2. In this effective potential, bound orbits have two turning points and a circular orbit corresponds to the special case where the particle*
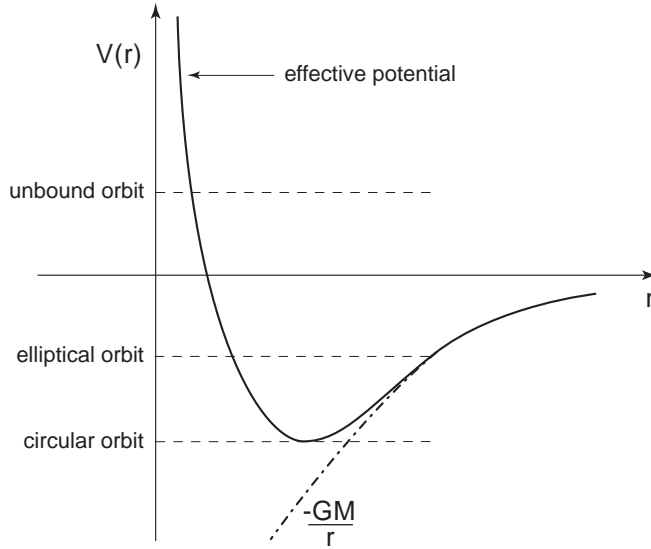
Figure 2. The Newtonian effective potential showing how an angular momentum barrier prevents particles reaching $r = 0$.

sits at the minimum of the effective potential. However, as we have already partially seen in equation (5.1), the same is not true in General Relativity.

Starting with equation (3.8) we can rewrite this as

$$\frac{1}{2}\dot{r}^2 + \frac{h^2}{2r^2}\left(1 - \frac{2GM}{c^2 r}\right) - \frac{GM}{r} = \frac{1}{2}c^2(k^2 - 1) \tag{3.20}$$

where we recall $k = E_{\text{part}}/mc^2$ and $r^2\dot{\phi} = h$.

Thus, although the r.h.s. is not the particle energy here, the fact that it is constant tells us that

$$U(r) = \frac{h^2}{2r^2}\left(1 - \frac{2GM}{c^2 r}\right) - \frac{GM}{r} \tag{3.21}$$

is an "effective potential" for the problem, which we can use to study stability in the same way as in the Newtonian case. Note that the relativistic term $(1 - 2GM/c^2 r)$ weakens the centrifugal effect of angular momentum at small r.

Differentiating this expression,

$$\frac{dU}{dr} = -\frac{h^2}{r^3} + \frac{3h^2 GM}{c^2 r^4} + \frac{GM}{r^2}, \tag{3.22}$$

and so the extrema of the effective potential are located at the solutions of the quadratic equation

$$GMr^2 - h^2 r + \frac{3h^2 GM}{c^2} = 0, \tag{3.23}$$

i.e. at

$$r = \frac{h^2}{2GM} \left\{ 1 \pm \sqrt{ 1 - 12 \left(\frac{GM}{hc} \right)^2 } \right\}. \qquad (3.24)$$

If $h = \sqrt{12}\frac{GM}{c}$ *there is only one extremum, and there are no turning points in the orbit for lower values of* h. *At this point* $r = 6GM/c^2 = 3R_s$. *Fig. 3 shows the effective*
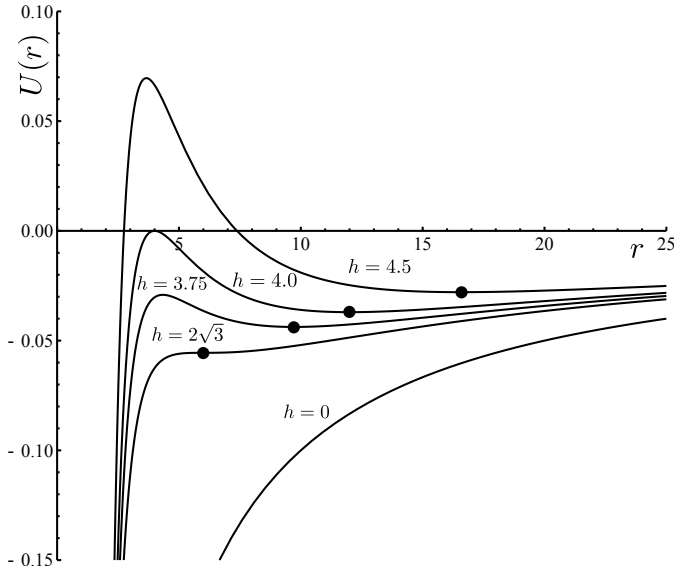
Figure 3. The effective potential $U(r)$ plotted for several values of the angular momentum parameter h (units here have $GM/c^2 = 1$).

potential for several values of h. *The dots show the locations of stable circular orbits. The maxima in the potential are the locations of unstable circular orbits.*

What is the physical significance of this result? The smallest stable circular orbit has

$$r_{\min} = \frac{6GM}{c^2}. \qquad (3.25)$$

Gas in an accretion disc settles into circular orbits around the compact object. However, the gas slowly loses angular momentum because of turbulent viscosity (the turbulence is thought to be generated by magnetohydrodynamic instabilities). As the gas loses angular momentum it moves slowly towards the black hole, gaining gravitational potential energy and heating up. Eventually it loses enough angular momentum that it can no longer follow a stable circular orbit and so it falls into the black hole. On this basis, we can estimate the efficiency of energy radiation in an accretion disc via looking at a plot of the 'fractional binding energy' $E/(mc^2) - 1 = k - 1$ *versus* r *(see Fig. 4).*

Bound energy for circular Schwarzschild orbit
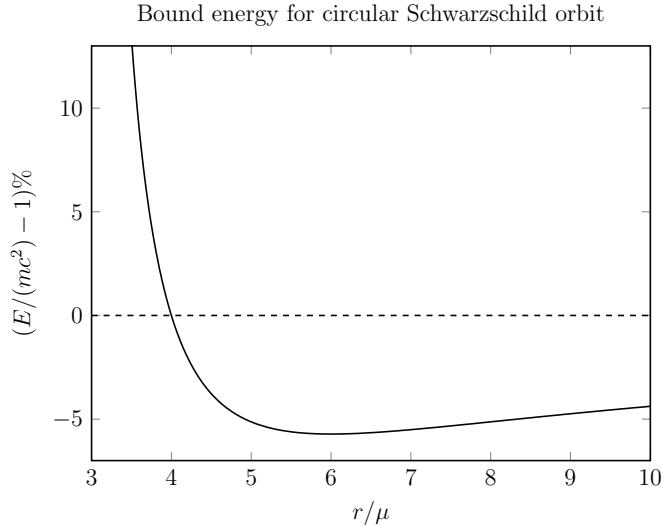
Figure 4. *A plot of $E/(mc^2) - 1$ in percent versus r (the latter measured in units of $\mu = GM/c^2$) where E is the energy of a particle of mass m in a circular orbit at radius r about a Schwarzschild black hole.*

The maximum efficiency is of order the gravitational binding energy at the smallest stable circular orbit divided by the rest mass energy of the gas. From the plot we can see that this will be about 6%. More accurately, from equation (3.14) we see that at $r = 6GM/c^2$ $k = E/(mc^2)$ is $2\sqrt{2}/3$, hence we obtain for this efficiency

$$\epsilon_{\mathrm{acc}} \approx 1 - 2\sqrt{2}/3 \approx 5.7\% \tag{3.26}$$

The equivalent Newtonian value, is not far away at

$$\epsilon_{\mathrm{acc}} \approx \frac{1}{2} \frac{GMm}{r_{\mathrm{min}}} \frac{1}{mc^2} \simeq \frac{1}{12} \sim 8\%. \tag{3.27}$$

As we will see, this value can be even larger for a black hole with spin, and an accretion disc can convert 5-20 percent of the rest mass energy of the gas into radiation, depending on spin. This can be compared with the efficiency of nuclear burning of hydrogen to helium (26 MeV per He nucleus),

$$\epsilon_{\mathrm{nuclear}} \sim 0.7\% \tag{3.28}$$

Accretion discs are capable of converting rest mass energy into radiation with an efficiency that is about 10 times greater than the efficiency of nuclear burning of hydrogen. The 'accretion power' of black holes causes the most energetic phenomena known in the Universe.

4 Evidence from X-rays, quasars and AGN

The early 1960s also saw the birth of X-ray astronomy, when in June 1962 Riccardo Giacconi and colleagues [25] launched a sounding rocket with Geiger counters sensitive to X-rays. As the detectors scanned across the Sky during their 10 minutes above the Earth's atmosphere, a broad peak of emission was discovered from the general direction of the Scorpius constellation and a steady background of cosmic X-rays were seen. Sco X-1 and the cosmic X-ray Background had been discovered. The rapidly variable X-ray source Sco X-1 is a neutron star accreting matter from an orbiting companion star and the X-ray Background is now known to be the integrated emission from accreting supermassive black holes at the centres of distant galaxies (see Fig. 5).
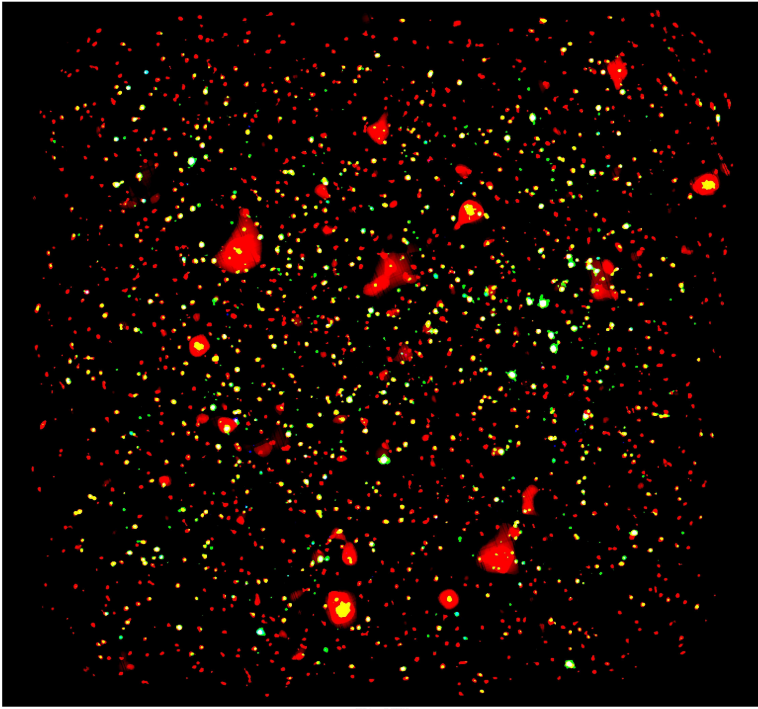
Figure 5. The XMM COSMOS field is about 30 arcmin across and shows the X-ray Background resolved into pointlike and extended X-ray sources. The pointlike sources are mostly accreting black holes (distant AGN) and the extended sources are due to hot gas pooled in the gravitational potential wells of clusters and groups of galaxies.

The first clear association of X-ray astronomy and black holes was made after Giacconi and colleagues studied the brightest X-ray source in the constellation of Cygnus, Cyg X-1, using the first X-ray astronomy satellite, Uhuru, which continuously scanned the Sky. Cyg X-1 showed chaotic variability on timescales down to a fraction of a sec-

ond. It has two relatively long-lived states, one when the spectrum is soft and the other hard. A radio source was found to appear when it switched into the hard state and accurate measurement of the position of that source enabled it to be identified with a 7th magnitude B star, HDE 226868. Separate teams of optical astronomers, Webster & Murdin [76] and Bolton [5], then found that this massive star was being swung around at $70\,\mathrm{km\,s^{-1}}$ by an unseen object on a 5.6 day period. This enabled mass estimates to be made (which relied on understanding the mass of the companion B star) yielding at least $3.5M_\odot$ which is above the likely upper mass limit for a neutron star of about $3M_\odot$. The small size implied by the rapid variability combined with the lower mass limit pointed to a black hole in Cyg X-1.

Many other black hole X-ray binary systems are now known, some of which have much clearer mass estimates. M33 X-1, for example, in the nearby galaxy M33 has a precise distance and stellar mass estimate and also shows eclipses which enable the orbital inclination to be deduced, leading to a mass for the X-ray source of $15.64 \pm 1.45M_\odot$ [51].

By the 1980s, many quasars and X-ray binary systems were known, showing that black holes are common. Quasars were seen to be an extreme part of the more general phenomenon of Active Galactic Nuclei (AGN). The centres of a few percent of all galaxies appear to have some non-stellar activity in the form of bright broad emission lines, a nonthermal radio source or an X-ray source. Quasars occur when the AGN outshines the host galaxy in the optical band. AGN of lesser power are known as Seyfert galaxies or just low luminosity AGN as the power drops. Jets of highly-collimated relativistically outflowing plasma are found in about 10% of AGN. An example outflow in one of the nearest AGN is shown in Fig. 6.

Unusual emission spectra at the centres of some galaxies had been known as a phenomenon since about 1908, and the first jet was reported in M87 by Heber Curtis in 1918 [12]. Little follow-up work was done before the 1960s, apart from Carl Seyfert's PhD thesis in the 1940s [64]. By the end of the 1980s most astronomers considered that AGN were powered by accretion onto black holes, but a minority still favoured some other explanation, such as multiple supernova outbursts. The arguments for black holes were strong but circumstantial. A major observational problem was that black holes are by definition difficult to observe directly.

Quasars appear to be associated with a past phase in the evolution of the Universe, when it was 1-5 billion years old (mostly at redshifts of 2-4). They are now relatively uncommon compared with that era. (3C273 is a rare quasar at low redshift: low is relative here as it was moderately high when discovered in the early 1960s.) The enormous powers involved mean that the accretion rates were high and the mass doubling time of the black holes could have been a few 100 million years. Radiation pressure would have restricted the inflow to below a limit first deduced for stars by Eddington, known as the Eddington limit. The limit is obtained by comparing the force of radiation acting on an electron (through Thomson scattering of cross-section σ_T) at the surface of the object, with the force of gravity on a proton there. The electron and proton, although
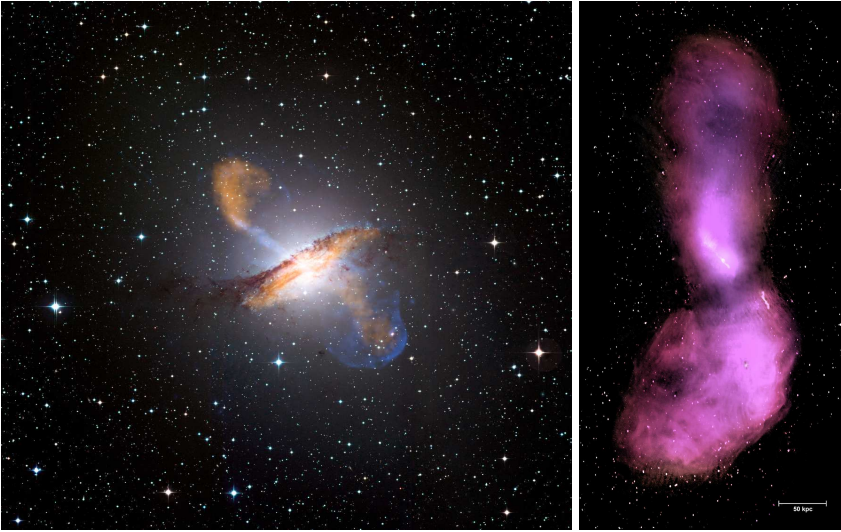
Figure 6. Centaurus A is one the nearest radio-loud AGN. The image on the left is a combination of infrared through X-ray images, its jets are seen going from the NE to SW. On the right is a larger scale image of low frequency radio emission showing the large diffuse lobes of radio-emitting plasma ejected by the accreting black hole out to intergalactic space.

assumed free, are bound together by electrostatic attraction.

$$F_{\text{grav}} = \frac{GMm_{\text{p}}}{R^2} = F_{\text{rad}} = \frac{L}{4\pi R^2 h\nu}\sigma_{\text{T}}\frac{h\nu}{c}, \tag{4.1}$$

where the radiative force term is the flux of photons (of typical energy $h\nu$) times the cross-section times the momentum of a photon. This gives

$$L_{\text{Edd}} = \frac{4\pi GMm_{\text{p}}c}{\sigma_{\text{T}}}, \tag{4.2}$$

which is about 10^{31} W per Solar mass.

Since the Eddington limit is proportional to the mass of the black hole the black hole mass can grow exponentially, if sufficient fuel is available. If growth is at the Eddington limit, the e-folding time of the black hole mass is about 4×10^7 yr. This timescale is sufficient for the typical massive black hole to have grown from stellar mass (say $30M_{\odot}$) but it does become challenging for the most distant billion Solar mass quasars found above redshift 6.

5 Sgr A*, the Black Hole at the Centre of the Milky Way

The evidence for the existence black holes changed though the 1990s owing to careful observations of the motion of stars moving around the centre of our own Milky Way

galaxy, first starting in 1991 by Reinhard Genzel and colleagues [23] using ESO tele-
scopes and later joined by Andre Ghez and colleagues [24] using the Keck telescopes.
An interesting picture of the technique used to achieve the required image stability for
this work is shown in Fig. 7.

Figure 7. The central stellar bulge of our Galaxy. A laser beam from one of the ESO
Very Large Telescopes points at the very centre where Sgr A* resides. This creates an
artificial star in the Earth's upper atmosphere which is used to stabilise images made of
the stars orbiting the central black hole.

Most stars, like the Sun, orbit the centre of the Galaxy at about $230\,\mathrm{km\,s^{-1}}$, but
within the innermost light year they move faster until at a distance of $2000r_{\mathrm{g}}$ from the
dynamical centre a star orbits at up to $3000\,\mathrm{km\,s^{-1}}$. The inferred mass within that orbit
is 4 million $M_\odot$ and the dynamical centre coincides with a strange radio source in the
constellation of Sagitarius long known as Sgr A*. It is also a flickering infrared and
X-ray source. No stellar emission which can be attributed to say a massive cluster of
normal stars is seen. The stellar orbits of dozens of stars there are known in 3D, both
from their apparent motions mapped in the plane of the Sky and from line-of-sight
Doppler shifts. The orbit of one of the closest stars, S2, is shown in Fig. 8 [26]. The
mass density within the innermost orbits exceeds $10^{18}M_\odot\,\mathrm{pc^{-3}}$ and there is nothing
known to Physics which can lie there other than a black hole. Clusters of stars, even
neutron stars, would interact and collide. The above lower limit on the mass density
of the central object is increased by a further 5 orders of magnitude when constraints
on the maximum size of Sgr A* obtained from millimetre band Very Long Baseline
Interferometry (VLBI) are included.

The origin of the young, massive stars which are bright enough to be tracked around
the Galactic Centre is not yet fully understood. The underlying stellar density there is

The orbit of S2 (1992-2013)
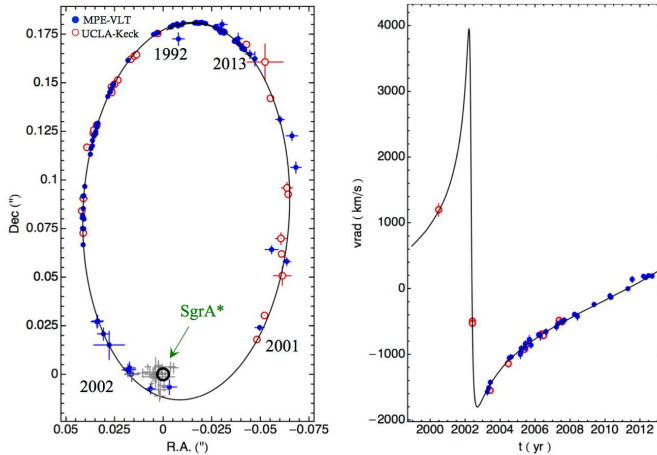
Figure 8. The path of star S2 about SgrA*. The elliptical orbit has a period of 15.2 years, a major axis of 5.5 light days and is inclined at 46 degree to the plane of the Sky. It requires that a mass of $4 \times 10^6 M_\odot$ lies within a radius of 17 light hours. The only long-lived object which is physically consistent is a massive black hole.

so high that it should inhibit further star formation.

As well as the issues of mass within a given radius, there is also hope that general relativistic effects on the orbits of stars and possibly gas clouds near Sgr A* will be observed in the near future, so we discuss now the details of these effects, including the important aspect of 'capture' by a black hole.

5.1   GR effects on orbits

We derived above the 'shape' equation for orbits around a Schwarzschild black hole, (3.9). For the Newtonian case, then due to the harmonic kernel at the left, and the constant at the right, it is obvious that solutions of the form $u = a + b \cos \phi$ will work, i.e. ellipses, so if the extra term in the relativistic version (3.9) is small we expect the orbits to be modified ellipses. In the Solar System, in which a Schwarzschild metric due to the Sun applies, these modifications are very small (e.g. the largest *effect is the 42 seconds per century precession of Mecury's orbit), but in the Schwarzschild metric around a black hole, we can expect much larger effects. For example, in Fig. 9 we show the motion for an object starting about 10 Schwarzschild radii out in an almost circular orbit. The gaps between the markers on the orbit are laid down at equal intervals of time, and so indicate how fast the object is moving. We can see that*

strongly precessing ellipses are obtained, but with a motion that looks as though it will continue indefinitely (which it does).

However, in Fig. 10, we show what happens when starting from the same point, and also moving tangentially, but now with a smaller specific angular momentum. This time, the object is clearly 'captured' by the black hole, and ends up crossing the black hole horizon.
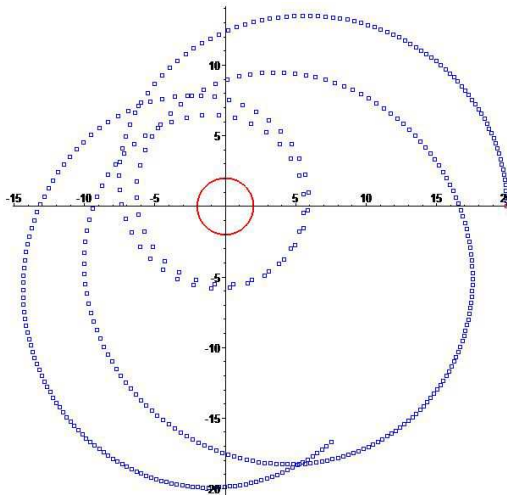
Figure 9. Advance of perihelion in a Schwarzschild metric. The units of distance are GM/c^2, where M is the mass of the central body. The particle is launched tangentially and given a specific angular momentum h of 3.75 where the circular orbit h would be 4.85. The circle marks the Schwarzschild radius of the central black hole.

We can gain some insight into how the 'capturing' comes about, by considering the orbit equation in a different form. For a massive particle, the interval s we have been using is just the proper time *of the particle, which we label τ. If we start with equation (3.8), differentiate with respect to interval τ and then remove first derivatives, $dr/d\tau$ using the original equation again, one arrives at the following:*

$$\frac{d^2r}{d\tau^2} = -\frac{GM}{r^2} + \frac{h^2}{r^3} - \frac{3h^2GM}{c^2r^4}. \qquad (5.1)$$

The first two terms are very Newtonian-like, and correspond to an inward gravitational force and a repulsive term, proportional to angular momentum squared, which is basically the 'centrifugal force'. What is new is the third term, also proportional to angular momentum squared, but this time acting inwards. This shows that close to the hole, specifically within the radius $r = 3GM/c^2$, centrifugal force 'changes sign', and is directed inwards, thus hastening the demise of any particle that strays too close to the hole, as in the example of Fig. 10.
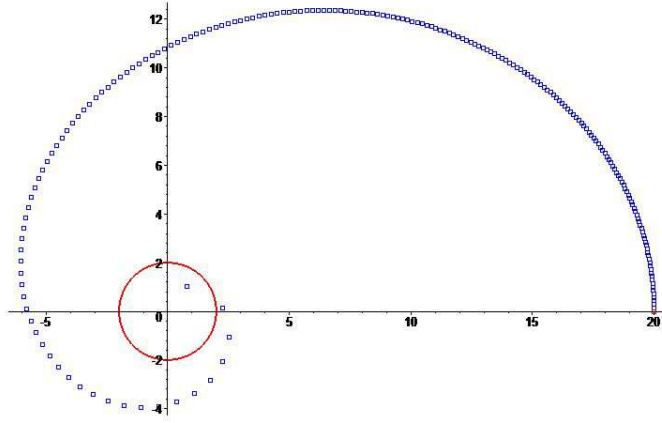
Figure 10. As for preceding figure but now for a particle projected with $h = 3.5$ (in units with $GM/c^2 = 1$).

Orbital precession

The equation we wish to solve is

$$\frac{d^2u}{d\phi^2} + u = \frac{GM}{h^2} + \frac{3GM}{c^2}u^2 \qquad (u \equiv \frac{1}{r}) \tag{5.2}$$

in the limit that the departure from Newtonian motion is small. This would apply to the motion of the planets in our solar system for example.

The Newtonian solution to this equation is

$$u = \frac{GM}{h^2}(1 + e\cos\phi), \tag{5.3}$$

and so we can use this as a first approximation, and then iterate to get a better one. Substituting into the r.h.s. of (5.2), we obtain the new equation

$$\frac{d^2u}{d\phi^2} + u = \frac{GM}{h^2} + \frac{3(GM)^3}{c^2h^4}(1 + e\cos\phi)^2. \tag{5.4}$$

This will be solved by $u = \frac{GM}{h^2}(1 + e\cos\phi)$ + the particular integral (P.I.) of the equation:

$$\frac{d^2u}{d\phi^2} + u = A(1 + 2e\cos\phi + e^2\cos^2\phi) \tag{5.5}$$

where $A = 3(GM)^3/c^2h^4$ is very small. The P.I. can be found to be:

$$A\left(1 + e\phi\sin\phi + e^2\left(\frac{1}{2} - \frac{1}{6}\cos 2\phi\right)\right). \tag{5.6}$$

Now, in this expression, the first and third terms are tiny, since A is. However, the second term, $Ae\phi\sin\phi$, might be tiny at first, but will gradually grow with time, since the ϕ part (without a cos or sin enclosing it) means it is cumulative. We must therefore retain it, and our second approximation is

$$u = \frac{GM}{h^2}(1 + e\cos\phi + \delta e\phi\sin\phi) \tag{5.7}$$

where

$$\delta = \frac{3(GM)^2}{h^2c^2} \ll 1. \tag{5.8}$$

Using

$$\cos(\phi(1-\delta)) = \cos\phi\cos\delta\phi + \sin\phi\sin\delta\phi \approx \cos\phi + \sin\phi\,\delta\phi \quad for \quad \delta \ll 1, \tag{5.9}$$

we can therefore write

$$u \approx \frac{GM}{h^2}\left(1 + e\cos[\phi(1-\delta)]\right). \tag{5.10}$$

u is therefore periodic, but with period $\frac{2\pi}{1-\delta}$. The r values thus repeat on a cycle which is slightly larger than 2π, and we find

$$\Delta\phi = \frac{2\pi}{1-\delta} - 2\pi \approx 2\pi\delta = \frac{6\pi(GM)^2}{h^2c^2}. \tag{5.11}$$

But from the geometry of the ellipse, and the Newtonian solution, where we know $l = h^2/GM$ and $l = a(1-e^2)$, we can get the final result:

$$\Delta\phi = \frac{6\pi(GM)^2}{c^2l(GM)} = \frac{6\pi GM}{a(1-e^2)c^2}. \tag{5.12}$$

For example, Mercury's orbit has $a = 5.8 \times 10^{10}$ m, eccentricity $e = 0.2$ and we know $M_\odot = 2 \times 10^{30}$ kg. Therefore our prediction for the precession is

$$\Delta\phi = 5 \times 10^{-7} \quad radians\ per\ orbit$$
$$= 0''.1 \quad per\ orbit.$$

Since Mercury's orbital period is 88 days, we would thus expect to accumulate a precession of $43''$ per century. This is what is observed after correction for the perturbations due to the other planets, which cause a total precession of more like $5000''$ per century.

Turning now to the Galactic Centre, the star S2, whose orbit was shown in Fig. 8, has an eccentricity of 0.876 and semi-major axis of 980 AU [16]. Taking the mass of the Galactic Centre black hole as $4 \times 10^6 M_\odot$, then our formula yields a precession of 11 arcmin per orbit, which takes about 15 years. This sounds large, but projected on the sky at perihelion amounts to only about 0.5 milliarcsec. By the use of near-infra red interferometry, this may be observable in the relatively near future (see Section 10), but as for the solar system it is competing effects from other nearby masses, and the general matter distribution near the centre, that will be key to determining whether it is the GR effect itself which is being seen [44].

6 AGN Feedback

It was earlier unclear whether galaxies with central black holes were special in some way or not. Quasars could be long lived in just a few galaxies or short lived and occur in every galaxy. Then careful imaging of the centres of nearby galaxies with HST and other telescopes revealed through the 1990s that most galaxies host a massive black hole. The mass of the black hole is correlated with the mass of the galaxy bulge[3] that it is embedded in (the Magorrian relation [37]). Current results indicate that the host bulge has a mass 500 times that of the black hole. Some argue that the correlation is better if the velocity dispersion of the surroundings stars (beyond the radius where the black hole's mass dominates) is used (the $M_{BH} - \sigma$ relation — an example of this is shown in Fig. 11).

Both correlations show considerable scatter but hold over several orders of magnitude.

The $M - \sigma$ relation poses the question of how the black hole at the centre of a galaxy knows the total mass of the host galaxy? The ratio of the physical size of the black hole event horizon to the galaxy can be 100 million or more (a similar scaled comparison is the Earth and a football). Some astronomers argue that larger galaxies just have larger black holes, but the correlations look better then that. An exciting possibility is that the question should be turned round and it is the black hole which controls the mass of the host galaxy. In 1998 Silk & Rees [66] proposed that it was the phenomenal energy output in the quasar phase, as the black hole grew in mass by accretion, which was responsible. Both grow from gas in the galaxy — the galaxy forming stars from the gas, the black hole accreting the gas. Eventually the black hole is so big and powerful that it blasts all the gas from the galaxy so both stop growing and we are left with the observed relation.

There is clear evidence that massive black holes have grown by accretion from the Soltan relation [67]:

$$\mathcal{E}_{\text{acc}}(1 + z) = \frac{\eta}{(1 - \eta)}\rho_{\text{BH}}c^2, \qquad (6.1)$$

---

[3] This means that the mass of any galactic disc is ignored.
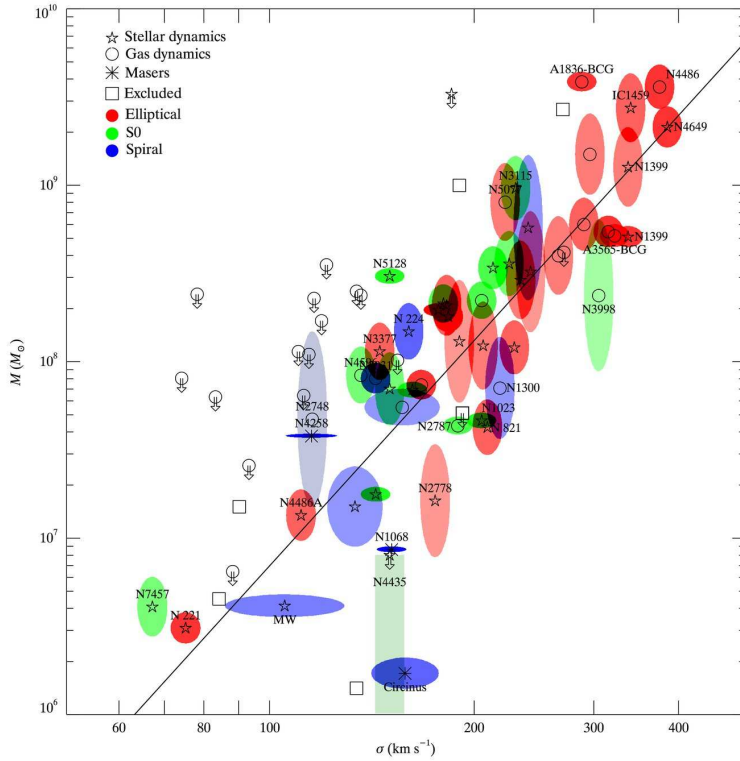
Figure 11. The black holes mass – stellar velocity dispersion relation $M_{bh} - \sigma$ [27]).

where z is the mean redshift at which the accretion occurs. It is a recasting of the famous equation, $E = mc^2$, in terms of densities. The factor of $1 + z$ is due to the redshifting of the energy of the radiation; there is no such factor for mass. η is the radiative efficiency of the accretion process $L = \eta \dot{M} c^2$. The energy density of radiation from accreting black holes, $\mathcal{E}_{acc}$ can be measured from the summed spectra of AGN (and the X-ray Background) and ρ_{BH} can be estimated from the mass function of galaxies together with the $M_{BH} - M_{gal}$ relation. Results show agreement if η is about 0.1 which, as discussed later, is typical for luminous accretion.

It is straightforward to show that the growth of the central black hole by accretion can have a profound effect on its host galaxy. If the velocity dispersion of the galaxy is σ then the binding energy of the galaxy bulge, mass M_{gal}, is $E_{gal} \approx M_{gal}\sigma^2$. The mass of the black hole is on average observed to be $M_{BH} \approx 2 \times 10^{-3} M_{gal}$. If the radiative efficiency of the accretion process of 10%, then the energy released by the growth of the black hole is given by $E_{BH} = 0.1 M_{BH} c^2$. Therefore $E_{BH}/E_{gal} \approx 2 \times 10^{-4}(c/\sigma)^2$. Very few galaxies have $\sigma < 350 \, \mathrm{km \, s^{-1}}$, so $E_{BH}/E_{gal} > 100$. The energy produced by the growth of the black hole therefore exceeds the binding energy of the host galaxy

by about two orders of magnitude!

If even a small fraction of the accretion energy can be transferred to the gas, then an AGN can have a profound effect on the evolution of its host galaxy. In practice, radiation from the accreting black hole will not have any significant influence on existing stars in the galaxy, It can however strongly influence gas clouds from which new stars can potentially form. By ejecting those clouds from the galaxy, AGN feedback can effectively stop further stellar growth of a galaxy.

The original mechanism of Silk & Rees is actually a little too effective and although it predicts a slope to the relation which is acceptable, the normalization is too low. Gas is blasted out too easily. However, energy is likely to be radiated away in the process which is likely to be controlled by conservation of momentum [18, 32, 45]. (Rocket science would be much easier if only energy conservation were at stake.) It has since been shown that this leads to the correct normalization and a slightly flatter slope. The details now centre [19] on the precise mechanisms responsible for the ejection (e.g. radiation pressure or accretion disc winds). Energetic winds are seen from some AGN and UV radiation interacts strongly with dusty gas in all quasars exerting an outward force through radiation pressure.

It is interesting to note that the effective Eddington limit for dusty gas exposed to the ultraviolet radiation of a quasar is about 500 times that of ionized gas such as expected close to the quasar. The $M - \sigma$ relation means that when the quasar is at its Eddington limit locally, the host galaxy is also at its effective Eddington limit globally.

Dramatic evidence of AGN feedback occurs in the cores of many clusters of galaxies. The intergalactic medium in clusters has been squeezed and heated by gravity to create an intracluster medium which is 10 million K or hotter. The baryons in the hot gas exceed all baryons in the galaxy members of the cluster by a factor of more than ten. The most massive galaxies known lie at the dense centres of clusters where accretion onto their massive black holes feeds energy into the intracluster medium, preventing it from cooling down due to the emission of X-rays. The total mass of gas in a cluster and the depth of the gravitational well is so large that the gas cannot be expelled. Energy instead flows from the black hole accretion process into the gas to maintain a themodynamic status quo.

The energy flows from the near vicinity of the black hole in the form of relativistic jets which push the hot gas back, forming giant galaxy-sized bubbles of relativistic plasma (cosmic rays and magnetic field) — an example is shown in Fig. 12.

The bubbles are buoyant and when large detach and float upward in the cluster potential, while new bubbles form and grow. The power in the bubbling process can be estimated from the energy content of a bubble ($4PV$ where P is the pressure of the surrounding gas and V is the volume of the bubble, the factor 4 being appropriate for relativistic plasma) divided by the bubble growth time. This power matches the radiative energy loss of the inner cluster core, indicating that close feedback has been maintained for billions of years [11].

AGN feedback implies that black holes play a central role in the final growth and
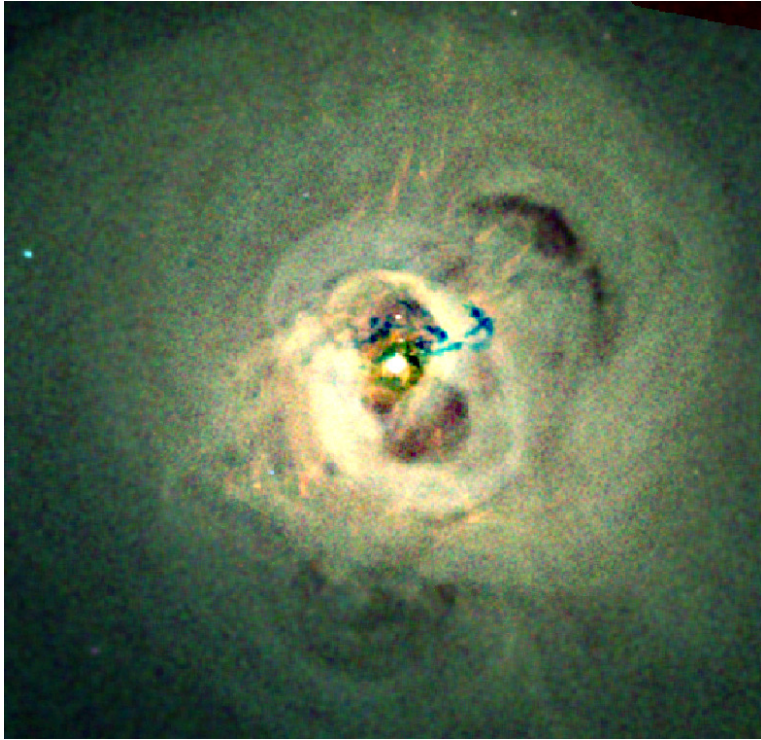
Figure 12. X-ray image of the core of the Perseus cluster centred on the giant galaxy NGC1275. The image is about 100 kpc or 300 thousand light years across. The AGN at the centre has blown 10 kpc diameter bubbles of relativistic plasma into the surrounding cluster gas. Detached buoyant bubbles are seen to the NW and S. Concentric ripples are seen in the hot gas due to the bubbling activity created by the AGN. It is clear that a black hole can have dramatic effects on gas structures both in and beyond the host galaxy.

evolution of all massive galaxies. If black holes did not exist then massive galaxies would be much larger and brighter than we now see.

6.1   Jets, Gamma-Ray Bursts and the Birth of Black Holes

Relativistic jets occur in about 10% of AGN and in low-state BHB. They are thus a marker of the presence of a black hole. The details of how the material is accelerated and collimated are still unclear, with possibilities discussed later in this Chapter. Apparent superluminal motion indicates that the bulk Lorentz factor in many jets $\Gamma \sim 10$. Polarization indicates that the radio and much other emission are due to synchrotron radiation. The jets therefore contain electrons and a component with positive charge is expected, unless the jets represent enormous currents. Whether the positive particles are positrons or protons is not known. If they are protons (or even heavier nuclei), then

the power in the jets can be huge, exceeding the radiative power in some objects.

Jets are presumably accelerated magnetically by the accretion disc. Fields emerging from the disc are continuously wound up around and along the central axis. The details are not yet fully understood. Jets are seen from all classes of object exhibiting accretion discs, including young stars and accreting white dwarfs. A long discussed possibility from quasar jets is that in some cases the spin energy of the black hole is being tapped by the Blandford-Znajek mechanism, which is a variant of the Penrose process (see Sections 12.5 and 12.7 below). There has been recent progress in successfully modelling jets using numerical simulations of this mechanism.

The most relativistic jets occur in Gamma-Ray Bursts (GRB). These were discovered in the late 1960s by the Vela spacecraft which had a gamma-ray detector to monitor the Cold War Test Ban Treaty (but not made public by Ray Klebesadel and colleagues from Los Alamos until 1973 [33]). They are intense flashes of gamma-rays which have a flux which would make them readily visible to the naked eye if in the optical band. Many theories of their origin were proposed, mostly based on neutron stars. It was not until the late 1990s that a GRB was localized and identified with a distant galaxy, by the BeppoSax satellite, that made it clear that GRB are the most luminous events in the Universe, representing about a Solar rest mass of energy radiated within a few 10s of seconds.

Luminosity and causality point to enormous concentrations of gamma-rays in a very small region which would instantly lead to electron-positron pair creation creating a electron scattering dense fog, preventing any radiation emerging. It is difficult to see how gamma-rays can be seen unless strong relativistic beaming, $\Gamma \sim 100$, is involved. Many aspects of GRB, including the radio through X-ray afterglow all support this highly relativistic interpretation [57]. The source of GRB must also be clean of any other matter, which could prevent the radiation emerging. It may then be surprising then that the source of GRB is now believed to be the very centre of dying massive stars as a black hole is formed. The swirling matter powers intense jets which burrow through and out of the star, to produce the GRB display. The birth of a black hole is therefore marked by one of the most amazing displays in the Universe.

Stars which give birth to black holes are estimated to start life at masses exceeding $25 M_\odot$. Such stars have luminosities which are a million times greater than the Sun and live for just a few million years.

7 Current Observations of Accreting Black Holes

Apart from the nearest examples, we know of the presence of most black holes from the power emitted as radiation and jets produced as a result of accretion. Matter falling into a black hole is accelerated by gravity up to the speed of light and if collisions occur then the matter can become very hot and radiate. The efficiency of the process depends on the rate of collisions and on whether the matter has time to radiate before falling into the event horizon. If the flow is a thin dense accretion disc then collisions

are plentiful and the efficiency depends on the ISCO (innermost stable circular orbit). Defining the radiative efficiency η through $L = \eta \dot{M} c^2$, then η ranges from 5.7% to 42% as the spin a/M increases from 0 to 1. In practice it is impossible to spin a black hole up to exactly 1, and high spins mean $\eta \sim 20 - 30\%$. Note that η for complete nuclear fusion (hydrogen to iron) is 0.7%, so black hole accretion is about an order of magnitude or more higher in efficiency. We now give some details of where these numbers come from, by looking at the orbits of massive particles around a Kerr black hole.

7.1 Particle motion in the Kerr metric

Before discussing the details of particle motion, we need to consider the general structure of the Kerr solution, since this determines the character of the regions in which the particles are able to move.

The most important regions for astrophysical purposes are shown in Fig. 13. We
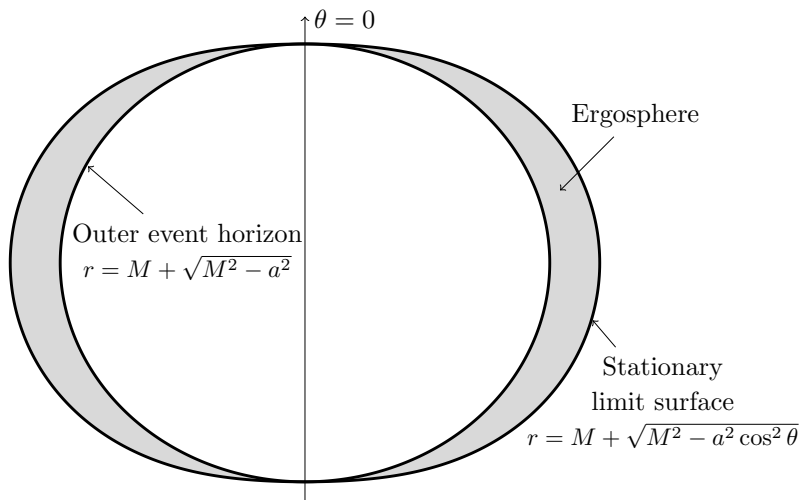
Figure 13. The stationary limit and outer horizon surfaces for the Kerr solution.

have drawn an outer surface, called the 'Stationary limit surface', and the one lying inside this is called the 'Outer event horizon'. Both of these are complemented by further surfaces (not drawn) lying closer to the black hole centre (the 'Inner Stationary limit' and 'Inner horizon' surfaces), but these are shielded by the outer horizon, and so do not have an immediate astrophysical role.

The stationary limit surface marks the point where it is no longer possible for an observer to remain stationary in the (r, θ, ϕ) coordinate system. Try as he or she

might, it is inevitable that they will be swept around by the rotation of the hole. Math-
ematically, this corresponds to the point where the g_t Killing vector corresponding to
invariance of the metric under time translations, changes from timelike to spacelike,
i.e. to where the g_{tt} component of the metric (3.1) passes through zero. This requires
(setting $c = G = 1$ for clarity in the expressions)

$$r^2 - 2Mr + a^2 \cos^2 \theta = 0, \quad i.e. \quad r = M \pm \sqrt{M^2 - a^2 \cos^2 \theta} \qquad (7.1)$$

and the outer of these surfaces is shown.

The other surface drawn corresponds to the point where the g_{rr} component of the
metric (3.1) becomes infinite, and marks the position of the event horizon. This is the
position from beyond which a particle can never escape, whatever its mass or state
of motion. It is different from the stationary limit, since particles in the inbetween
region, although they cannot remain stationary, can in principle escape to infinity.
This inbetween region is known as the 'ergosphere', since it is possible to arrange
particle motions so that work can be extracted from it (see Section 12.5 below). The
position of the horizon itself can be found by requiring

$$\Delta = r^2 - 2Mr + a^2 = 0, \quad i.e. \quad r = M \pm \sqrt{M^2 - a^2} \qquad (7.2)$$

and again the outer of these two surfaces is shown. Given that this radius, unlike the
stationary limit surface, does not depend on θ, it might be wondered why the surface
is drawn oblate in the diagram. This is because that Boyer-Lindquist coordinates do
not correspond to spherical polars even in the case where the mass vanishes, and
an embedding of the 2d surfaces we are working with into Euclidean space (for the
purposes of visualisation) results in ellipsoids even for $r = $ const. — see Section 13.6
of [30] for details.

The Lagrangian methods used above in the Schwarzschild case also work here,
and one finds quickly the following results for the $\dot{t}$ and $\dot{\phi}$ of a particle moving in
the equatorial plane in terms of its conserved specific energy and specific angular
momentum, k and h:

$$\dot{t} = \frac{k\left((r + 2M)a^2 + r^3\right) - 2haM}{r\Delta}$$
$$\dot{\phi} = \frac{h(r - 2M) + 2kaM}{r\Delta} \qquad (7.3)$$

As before, for the $\dot{r}$ equation it is simpler to use the fact that evaluated numerically
the interval function $G(x^\mu, \dot{x}^\mu)$ is 1 for a massive particle, and 0 for a photon. We
start with discussing a massive particle, since our initial emphasis is on the energy
liberated from accretion disc orbits. Here we find

$$\dot{r}^2 = k^2 - 1 + \frac{2M}{r} - \frac{1}{r^2}\left(h^2 - a^2(k^2 - 1)\right) + \frac{2M}{r^3}(h - ak)^2 \qquad (7.4)$$

We now have three equations we can integrate to find the motion. A key quantity for the energy and stability is the effective potential in r. We define this similarly to before via

$$\frac{1}{2}\dot{r}^2 + U_{\text{kerr}}(r) = \text{const.} \tag{7.5}$$

resulting in

$$U_{\text{kerr}}(r) = -\frac{M}{r} + \frac{1}{2r^2}\left(h^2 - a^2(k^2-1)\right) - \frac{M}{r^3}(h-ak)^2, \tag{7.6}$$

where an irrelevant overall constant has been ignored.

If we compare with the equivalent in the Schwarzschild case, equation (3.21), we can see that despite the increased complexity of the Kerr metric, the effective potential has terms in just $1/r$, $1/r^2$ and $1/r^3$ as before, resulting in overall similar behaviour (at least for small a). A difference, however, is that now the coefficients of the second and third terms depend on the particle energy as well as the angular momentum.

For a circular orbit, we can use the fact that $\dot{r}$ and $\ddot{r}$ are zero to find expressions for the specific energy and angular momentum. For the prograde orbits we are currently considering, these turn out to be

$$k = \frac{1 - \frac{2M}{r} + a\sqrt{\frac{M}{r^3}}}{\sqrt{1 - \frac{3M}{r} + 2a\sqrt{\frac{M}{r^3}}}}, \quad h = \frac{\sqrt{Mr} - \frac{2aM}{r} + a^2\sqrt{\frac{M}{r^3}}}{\sqrt{1 - \frac{3M}{r} + 2a\sqrt{\frac{M}{r^3}}}} \tag{7.7}$$

An important quantity for us to find is the radius of the innermost stable circular orbit, expected to be the inner edge of an accretion disc around a Kerr black hole, and the value the energy function takes there.

As in the Schwarzschild case, we can use the effective potential to do this, asking that its second derivative is positive where the first derivative vanishes. Calculating this for the $U(r)$ in (7.6) leads to the relatively simple criterion for stability

$$r^2 - 6Mr + 8a\sqrt{Mr} - 3a^2 > 0 \tag{7.8}$$

This is soluble analytically for r, but perhaps more illuminating to is to look at a plot of r_{ISCO} (the r corresponding to the innermost stable circular orbit) versus spin, as shown in Fig. 14. If $a = M$, an 'extremal' black hole, then the solutions are $r = M$ and $r = 9M$. If $a = 0$, we get the single solution $r = 6M$ corresponding to the Schwarzschild case. The former of these shows that stable circular orbits (in the prograde direction) persist right up to the event horizon for a black hole spinning at the maximum mathematically allowed rate, i.e. $a = M$. We note, however, that various effects are likely to intervene before this maximum spin rate can be achieved (mainly the counteracting torque felt by the hole in absorbing radiation from the accretion disc [70]), and $a = 0.998M$ is considered the most likely maximum attainable value, leading to a minimum attainable r_{ISCO} of $1.24M$.
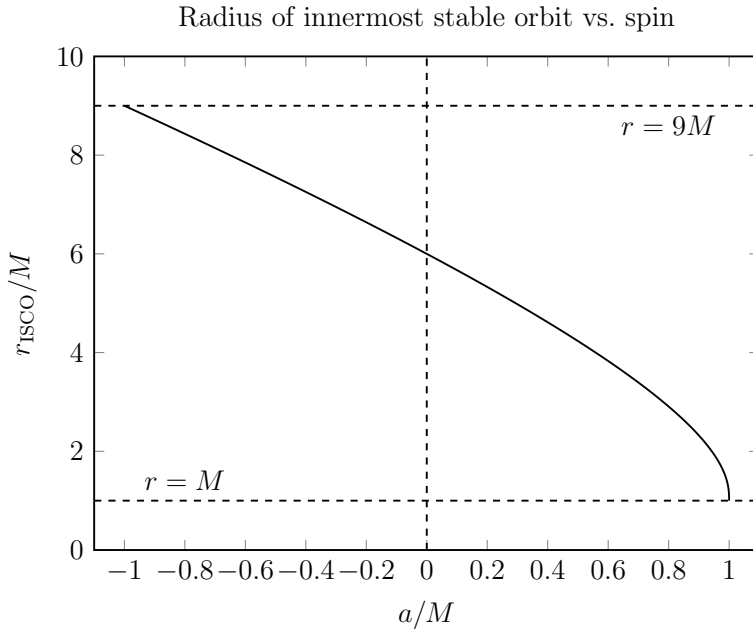
Figure 14. Plot of radius of innermost stable orbit vs. spin.

More generally, by eliminating r between (7.8) and the expression for k in (7.7) we can get a useful relation between the black hole spin and the efficiency of energy release for a particle which has reached the ISCO. For prograde orbits this relation is

$$\frac{a}{M} = \frac{2\left(2\sqrt{2}\sqrt{1-k^2} - k\right)}{3\sqrt{3}(1-k^2)} \tag{7.9}$$

This provides the plot of efficiency versus spin shown in Fig. 15. Again taking the maximum attainable value of a/M as 0.998, this leads to a maximum attainable efficiency of 32%.

7.2 Current Observations of Accreting Black Holes contd.

The accreted matter can be supplied by a companion star, in the case of a BHB, or from surrounding gas in AGN. How much is captured by the black hole in the AGN case will depend on the density, temperature, magnetic field and angular momentum of the gas. The case when there is no angular momentum and magnetic fields can be ignored is known as Bondi accretion, which assumes that the gas can be treated as a fluid. Basically gas within the Bondi radius, defined as the radius beyond which the

Efficiency of energy release vs. spin
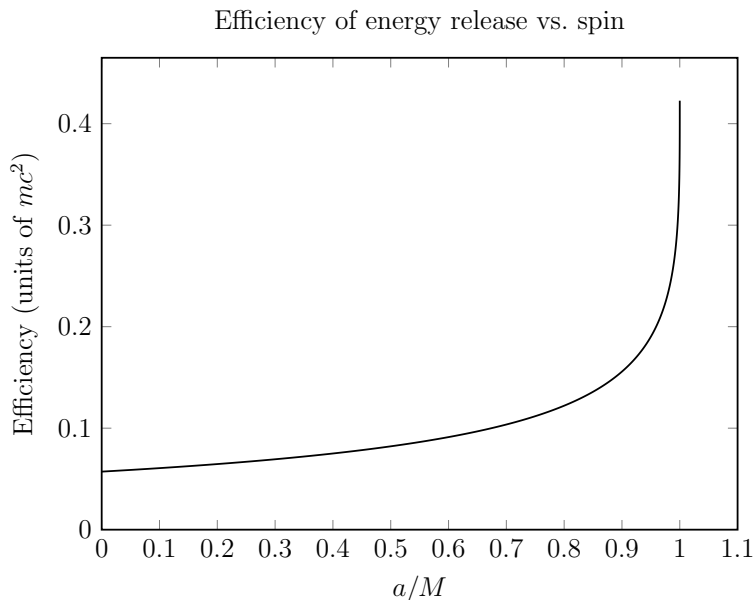
Figure 15. Plot of efficiency of energy release vs. spin (prograde orbits).

gas particles have the escape velocity, will be captured and this can be many orders of magnitude larger then would occur if the particles were free particles with no interactions or collisions. Zero angular momentum is a rather extreme assumption and may not apply to any real system, but it presents an easily calculated order of magnitude estimate of the accretion rate. Angular momentum is likely to reduce any inflow rate and could even choke off the flow. Indeed accretion flows can be unstable when heating by radiation from the central accreting mass is considered. Magnetic fields and turbulence also contribute to complexity and accretion flows are commonly observed to show chaotic variability.

The accretion disc will be thin, with the ratio of thickness to radius, $h/r < 0.1$, when the luminosity is above about 1% L_{Edd}. At lower accretion rates the disc thickens as the collision rates drop which can then cause the efficiency to drop with further decreases in $\dot{M}$. (The black hole swallows both the matter and energy released.) The properties of such radiatively inefficient flows (RIAFS) depend on whether the electrons (which radiate) and the protons (which have much of the energy) remain coupled, i.e. have the same temperature. There are still theoretical issues remaining as to whether this happens in such a highly magnetized plasma, but observations do indicate changes in behaviour in objects with low accretion rates. Not least is a tendency for jets to become common. The low luminosity of Sgr A* suggests it is in an extreme RIAF state.

The luminous accretion flows, however, are usually above 1% L_{Edd} and so are thin and dense and optically thick resulting in much radiation being emitted as a black body. The spectrum of the disc is then produced by the sum of blackbodies from different radii which gives a $\nu^{-1/3}$ spectrum at low energies up to the highest energies, which come from the smallest radii, where it turns over into a Wien tail. The peak temperature scales as $\dot{M}r_g^{-1/4}$. This means that the most massive luminous black hole systems have spectral peaks in the UV, while stellar mass black holes peak in the X-ray band.

Significant power can also emerge as a results of magnetic fields wound up in the accretion flow. They can emerge from the disc, become twisted and create a mess of reconnecting field lines powering a hot corona, with a temperature which can easily be 100 times hotter then the disc itself. The million degree Solar corona with associated flares and outflows is a nearby example but even low luminosity AGN have a power 10^{12} times larger than the Sun, so the analogy should not be taken too literally. The corona is the source of most of the X-rays seen from AGN. Evidence discussed later indicates that the corona in bright objects is located above and close to the black hole ($\sim 10 r_{\text{g}}$). The magnetic field structure also appears to power jets in some objects, and outflows in others. The degree to which the spin of the black hole is important (and maybe also a small ISCO) are still debated.

BHB have stellar-mass black holes and accrete from their companion star. Disc formation is implicit due to the orbital angular momentum. A few sources such as Cyg X-1 are persistent, with their long-term luminosity varying by less than an order magnitude, but sometimes switching states from hard (coronal dominated) to soft (thermal disc dominated). Many of the BHB are however transient, having outbursts every few years or decades, during which the luminosity can rise from 10^{33} to 10^{39} erg s^{-1} . Outbursts follow a similar pattern in the luminosity-colour (hardness) plane, starting hard as the luminosity builds up towards L_{Edd}, then switching to being soft as the thermal disc emission dominates over the corona, before subsiding back to the hard state as they decline to quiesence [59]. At the peak of an outburst the nearest of these sources (eg A0620-00 at 2.5 kpc) can become the brightest in the sky, outshining Sco X-1 and even the Sun (except when it is flaring) by a large factor.

There are also many similar X-ray binaries in our Galaxy which host a neutron star instead of a black hole. We know about the neutron star by observation of rapid pulsations due to the spin of the highly magnetic field, or from X-ray bursts which are thermonuclear flashes taking place very near the neutron star surface. Many of these are also transient and behave in a similar way to BHB. The depth of quiesence has been proposed as evidence of an event horizon in BHB by Ramesh Narayan and colleagues [47]. Black holes have no hard surface and can accrete matter and radiation whereas neutron stars must emit the gravitational energy released. BHB generally have lower quiesent luminosities than neutron star binaries which fits in with this picture. Whether these systems have similar enough accretion rates in quiesence for this to be a proof has yet to be determined.

Both BHB and some neutron star systems also show quasi-periodic oscillations, discovered by Michiel van der Klis in 1986 [74]. This phenomenon is complex and may be a rich source of information about the accretion flow and geometry, but it has yet to be fully understood and interpreted. To understand at least one of the frequencies we would expect to be seen, we now calculate the expected orbital frequency seen by a distant observer for material in the innermost orbit.

7.3 Velocities and frequencies

For astrophysical black holes, further important quantities for circular orbits are the velocity in the orbit, and the orbital period. For the former, the velocity determines (essentially via special relativistic effects) an important component of the shift in frequency which occurs for line radiation coming from the accretion disc, and for the latter, we can in some cases see directly the modulation of radiation associated with an orbital period. These are thought to provide one of the frequencies within the 'quasi-periodic oscillations' which are occasionally observed from accreting stellar mass black holes and can have frequencies in the several hundred Hz region [74].

Working with a Schwarzschild black hole, then if we let v be the 'ordinary' velocity in a circular orbit, and α be the corresponding 'rapidity', then (temporarily dropping factors of c since this makes the formulae clearer), we have

$$v = \tanh\alpha \quad and \quad r\dot\phi = \gamma v = \sinh\alpha \tag{7.10}$$

We can thus use (3.11) for h and the definition $r^2\dot\phi = h$, to calculate v as a function of r, obtaining the simple result

$$v^2 = \frac{GM}{r - 2GM} \tag{7.11}$$

For an object rotating in the innermost stable circular orbit (ISCO), at $r = 6GM$, we therefore find that its velocity is half the speed of light. (Note that, perhaps surprisingly, exactly the same velocity is obtained for the ISCO about a spinning black hole with any magnitude for its spin.)

As regards orbital frequency, then since the t coordinate is the time as measured by a stationary observer at spatial infinity, if we can form $d\phi/dt$ then setting this equal to $2\pi\nu_{orb}$ will immediately give us the orbital frequency, in Hz, as measured by an external observer.

Thus using

$$\frac{d\phi}{dt} = \frac{d\phi}{d\tau}\frac{d\tau}{dt} = \frac{\dot\phi}{\dot t}, \quad \dot\phi = \frac{h}{r^2} = \sqrt{\frac{GM}{r^3}\frac{1}{(1 - \frac{3GM}{r})}} \tag{7.12}$$

and

$$\dot t = \frac{k}{1 - \frac{2GM}{r}} = \frac{1}{\sqrt{1 - \frac{3GM}{r}}}, \tag{7.13}$$

we find

$$\frac{d\phi}{dt} = 2\pi\nu_{\rm orb} = \frac{\dot{\phi}}{\dot{t}} = \sqrt{\frac{GM}{r^3}},$$

which despite being derived in full GR is exactly the Newtonian (Keplerian) result.

As an example, evaluating at the innermost stable circular orbit, $r = 6GM/c^2$, for a 10 solar mass black hole, yields the impressively high result of $\nu_{\rm orb} = 218$ Hz. Thus an emitting blob orbiting at this radius could potentially produce this frequency in the frequency spectrum of the source.

7.4 Further AGN properties

AGN range in luminosity from below 10^{10} to $10^{14}\,{\rm L}_\odot$ and are situated at the centre of the host galaxy. They appear to respect the Eddington limit and show strong evolution in luminosity with redshift (and thus cosmic time). The quasar and therefore mass-building phase peaked at about redshift 2.5 with quasars being observed back to redshift 7.1. An important issue with AGN is that a plentiful supply of fuel leads to obscuration of the source itself. If the absorbing column density is Thomson thick (ie most photons are scattered by electrons on passing out of the source), then only heavily reprocessed emission is all that remains, emerging predominantly in the infrared.

Type I AGN are largely unobscured and Type II obscured. The difference may be geometrical and due to our line of sight. In a broad class of source the obscuring medium is in the form of a thick torus at a radius of about a parsec. If viewed in the plane of the torus we see a Type II obscured object and if we view it face-on then it is Type I. If at the same time there is a jet, then face-on down the jet the object appears highly beamed as a blazar [72].

8 Measurements of the Masses of Black Holes

The mass of a compact object can be measured from the motions of stars or gas in its vicinity using Newton's Law of Gravitation. If a star makes a circular orbit around a massive black hole with velocity v at radius r then the mass of the black hole $M = v^2 r/G$. Multiplying factors emerge for different shaped orbits but the essence of measuring velocity and radius remains the same. For the black hole at the centre of our Galaxy, Sgr A*, the 3D motion of many nearby stars has been mapped to give the best estimate of $4 \times 10^6 M_\odot$.

With stellar mass black holes orbiting a normal star, then constraints on the mass are obtained by measuring periodic doppler shifts of spectral lines of that star to yield its radial velocity curve of semi-amplitude K and period P. These are combined to give the mass function

$$f = \frac{(M_{\rm bh}\sin i)^3}{(M_{\rm s} + M_{\rm bh})^2} = \frac{PK^3}{2\pi G} \tag{8.1}$$

Further progress requires estimates of the mass of the normal star, perhaps from its spectral type, and of the inclination of the orbit i. If the system is eclipsing then i must be high, but if not then other means must be used such as observation of periodic ellipsoidal variations in the lightcurve of the star due to tidal distortions. These can be modelled to yield the inclination. There are now several dozen black holes with masses estimated to about 10% in this manner.

The mass of supermassive black holes (SMBH) is obtained from the motions of nearby stars and gas if they lie in relatively nearby galaxies where the region of influence of the black hole can be resolved. This is roughly the radius within which the black hole-induced motions are faster than the general motions in the galaxy. The masses of more distant active SMBH can be determined using the reverberation technique. Delayed variations in the ionizing UV radiation from the nucleus are seen in orbiting broad-line clouds — the whole system appears to reverberate with delays ranging from days to weeks. (The clouds show doppler-broadened emission lines due to orbiting close to the SMBH.) The light travel-time delay then gives the radius and the line width of the clouds gives the velocity required to determine the central mass. Assumptions need to made about the geometry but careful work of the past two decades has established the success of the method [55]. It has enabled correlations to be built between the width of selected emission lines, optical luminosity and black hole mass.

Current results indicate a maximum mass for observed neutron stars at just over $2M_\odot$, while stellar mass black holes have masses from $\sim 4 - 20M_\odot$, with an average of about $7M_\odot$. Observed supermassive black holes have masses ranging from just below 10^6 to $2 \times 10^{10}M_\odot$. It is possible that some UltraLuminous X-ray sources (ULXs), which have luminosities greater than the Eddington limit for a $10M_\odot$ black hole, are Intermediate Mass Black Holes (IMBHs) with masses of $10^2 - 10^5 M_\odot$.

9   Measurements of Black Hole Spin

Whilst mass measurements can be made at a large distance from an object, spin requires a probe which is close in, within $10r_\mathrm{g}$[4]. The standard approach is to identify the inner edge of the accretion disc with the ISCO and then convert that radius to spin. This means that the inner disc must be luminous and detectable.

Bright Galactic X-ray binaries in the soft state generally have a quasi-blackbody X-ray spectrum which can be used to measure the emitting area using the Stefan-Boltzmann law in an analogous way to that by which stellar radii are determined (blackbody luminosity $L = 4\pi R^2 \sigma T^4$) [39]. Unlike the surface of a star, an accretion disc is not all at the same temperature, so the emission profile of the disc must be assumed and the black hole mass and distance determined in order to measure the ISCO and thus spin.

---

[4] If the mass accretion rate can be measured (from observations of the outer disc, say) and the total luminosity is known, then in principle spin can be deduced from the radiative efficiency using the relation in Fig. 15.

Light bending effects are very significant for the accretion disc near a black hole [43], so we now give some details of light bending effects in GR, first in the Schwarzschild metric, and then for Kerr black holes. An impression of what we would actually see for the accretion disc around a Schwarzschild black hole, if sufficient resolution was available, is shown in Fig. 16.
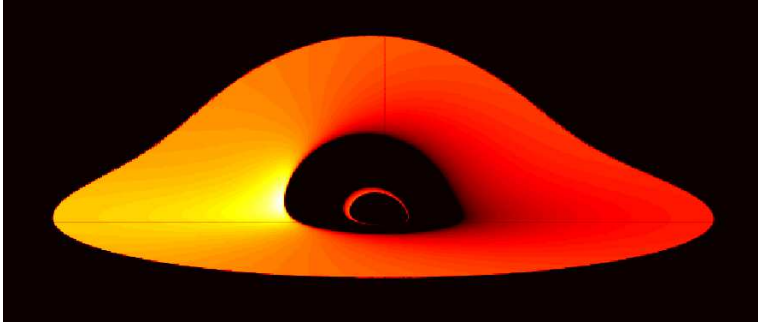
Figure 16. Pseudoimage of a luminous thin accretion disc around a black hole with doppler and gravitational redshift effects included. Light bending causes the distant side of the disc to appear as an arch above the hole. The smaller loop near the centre is due to scattering of photons from the (unstable) photon orbit at $r = 3GM/c^2$. The colour scale indicates flux received.

This can be compared with the more distorted and asymmetric image we would see from a black hole rotating at the expected maximum rate of $a = 0.998M$, in Fig. 17.
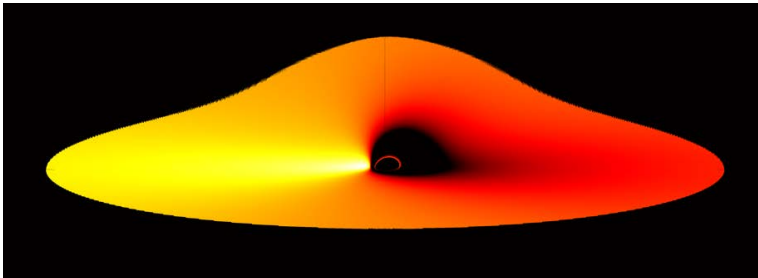
Figure 17. As for Fig. 16, but for a Kerr black hole rotating at the maximum attainable value of $a = 0.998M$ (see Section 7.1). The unstable photon orbit is now near $r = GM/c^2$.

9.1 Equations for photon motion and redshift

The other results we need for understanding astrophysical aspect of black holes, are the equations of motion for photons, and results for how their energy changes during propagation.

For the equations of motion, we can use the above analysis, but with the interval function $G(x^\mu, \dot{x}^\mu)$ set equal to 0 rather than 1, once its functional variation has been taken.

Tracking through the changes this causes, we find equation (3.8) is replaced by

$$\dot{r}^2 = k^2 c^2 - \frac{h^2}{r^2}\left(1 - \frac{2GM}{rc^2}\right) \tag{9.1}$$

and for the 'shape' equation, (3.9), one finds that it is now the 'Newtonian' term that disappears on the r.h.s., and we just get

$$\frac{d^2 u}{d\phi^2} + u = \frac{3GM}{c^2} u^2. \tag{9.2}$$

One can immediately confirm from this equation that there is a circular photon orbit at $r = 3GM/c^2$, as mentioned above, but is it stable?

To do the stability analysis, we rewrite the energy equation as

$$\frac{\dot{r}^2}{h^2} + V_{\text{eff}}(r) = \frac{1}{b^2}, \tag{9.3}$$

where $b = h/ck$, $\mu = GM/c^2$ and the effective potential

$$V_{\text{eff}}(r) = \frac{1}{r^2}\left(1 - \frac{2\mu}{r}\right). \tag{9.4}$$

Let us look at a plot of this function, Fig. 18. We can see $V_{\text{eff}}(r)$ has a single maximum at $r = 3\mu$ where the value of the potential is $1/(27\mu^2)$. This shows that the circular orbit at $r = 3\mu$ is unstable and in fact no stable circular photon orbit is possible in the Schwarzschild geometry.

Another immediate use of equation (9.2) is in connection with light bending. Referring to Fig. 19, we can see that a suitable first solution in which the term $3GMu^2/c^2$ is completely ignored, is

$$u = \frac{\sin\phi}{R}, \tag{9.5}$$

where R is the radius of the body the gravitational deflection due to which we wish to work out. We iterate this equation by putting $\sin^2\phi/R^2$ for u^2 on the r.h.s. of (9.2), i.e.

$$\frac{d^2 u}{d\phi^2} + u = \frac{3GM}{c^2 R^2}\sin^2\phi. \tag{9.6}$$

This is satisfied by the particular integral

$$u_1 = \frac{3GM}{2c^2 R^2}\left(1 + \frac{1}{3}\cos 2\phi\right), \tag{9.7}$$

Effective potential for photon motion
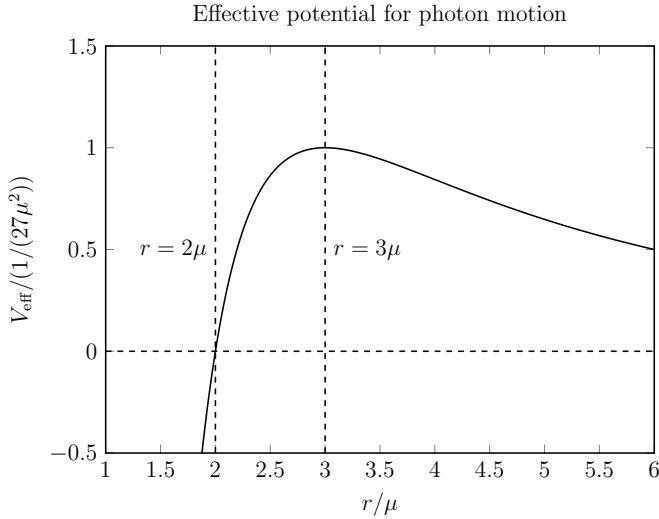
Figure 18. Plot of the effective potential for photon motion in the Schwarzschild geometry. (Units of V_{eff} are $1/(27\mu^2)$ where $\mu = GM/c^2$.)
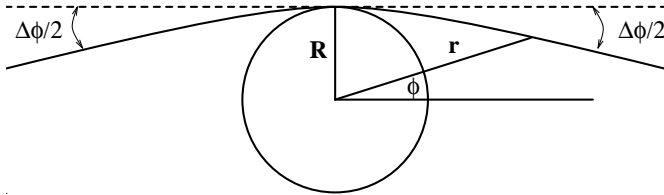
Figure 19. *Gravitational deflection of light*

and adding this into the original solution yields

$$u = \frac{\sin \phi}{R} + \frac{3GM}{2c^2 R^2} \left(1 + \frac{1}{3} \cos 2\phi \right). \tag{9.8}$$

Now consider the limit $r \to \infty$, i.e. $u \to 0$. Clearly we can take $\sin \phi \approx \phi$, $\cos 2\phi \approx 1$ there, and we obtain $\phi = -2GM/(c^2 R)$ so that the total deflection (see figure) is

$$\Delta\phi = \frac{4GM}{c^2 R}. \tag{9.9}$$

This is the famous gravitational deflection formula. For the Sun it yields 1.77 seconds of arc, and was first verified in the 1919 eclipse expedition. More recent high precision tests use radio sources, *since these can be observed near the Sun, even when there is no eclipse, and there is now no doubt that the GR prediction (which incidentally is*

twice what had previously been worked out using a Newtonian approach) is accurate to a fraction of a percent.

In the black hole context, much stronger bending can occur, for which this first approximation is insufficient, and the full equations of motion need to be integrated. This can lead to some interesting effects, illustrated below in the context of a Kerr black hole.

The other important aspect to discuss is gravitational redshift. Quite generally, for a metric with a Killing vector field g_t, the redshift due to gravitational time dilation will be given by the ratio of $p \cdot g_t$ at emission and reception, where p is the photon 4-momentum. g_t becoming null, i.e. g_{tt} going to zero, marks the point where infinite redshift is possible since p can then be in the direction of g_t, e.g. for counter-rotating photons at the Kerr Stationary limit. This redshift from $p \cdot g_t$ acts multiplicatively on any further redshifts which are occurring at a point due to special relativistic effects. E.g. for a point in an accretion disc, there will be a doppler redshift due to its motion relative to the initial path of an emitted photon, and then this will be multiplied by the gravitational redshift the photon experiences between that point and infinity. The combined effects of the redshifts can be seen in pattern of received flux seen in Figs. 16 and 17, which are for the case where the accretion disc itself has constant emissivity.

9.2 Light bending around a Kerr black hole

The treatment of photon orbits for the Kerr case can proceed in the same way as in Section 7.1, which dealt with massive particles, except that now the interval function $G(x^\mu, \dot{x}^\mu)$ evaluates to 0 instead of 1. Several textbooks, e.g. [30] and [22], deal with the details of the resulting orbits, and in particular show that as in the Schwarzschild case, there are still no stable circular photon orbits.

The possible orbits for non-equatorial photons can be quite exotic. As an example, we show in Fig. 20 the path of a photon emitted from an accretion disc in the equatorial plane, moving towards the black hole but with an initial upward component to its velocity. This moves round behind the black hole and is eventually able to escape to infinity, moving in a roughly opposite direction to its initial motion. This example is for a Kerr black hole with the maximum expected value for a of $0.998M$ — the ISCO and horizon radii are also shown.

9.3 Iron Line Emission

The method discussed above for Galactic X-ray binaries does not work for AGN since the much higher black hole mass means that the blackbody disc emission emerges in the far UV band which is unobservable because of absorption by Galactic hydrogen clouds. Observations are made instead of broad iron-line emission produced by X-ray reflection. This is the fluorescent and back-scattered emission produced by irradiation
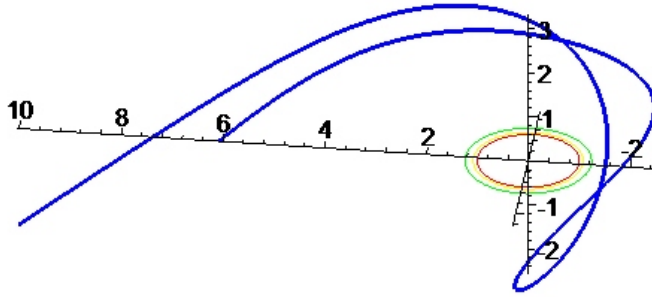
Figure 20. *Path of a photon emitted from an accretion disk that eventually escapes from the black hole in a direction about 180° from its initial direction.*
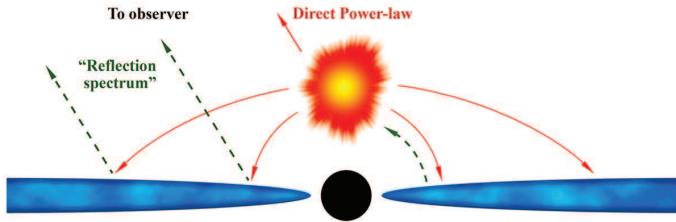
Figure 21. Schematic cross-section of an accretion disc around a black hole with a central corona providing irradiation. The production of the reflection spectrum is illustrated.

of the disc by the coronal X-ray continuum — see Fig. 21. X-rays absorbed in the disc lead to line emission, particularly iron K emission at 6.4 to 6.95 keV, depending on the ionization state of the emitter. At higher energies the X-rays are more likely to be Compton-scattered back out of the disc rather than absorbed, producing what is called the Compton hump in the reflection spectrum.

The spectral features are produced in the innermost parts of the accretion disc where gravitational effects are strong and lead to large doppler shifts and gravitational red-shifts which skew and broaden emission lines [21, 20] — an example is shown in Fig. 22. Detailed modelling of the line shape, and generally the shape of the whole observed reflection spectrum, leads to an estimate of the inner radius of the disc and thus the spin. Radii are determined in this method directly in gravitational units so the distance and mass of the black hole are not required.

The broad iron line method can also be used in certain states of BHB [42] and has been found to give consistent results with the blackbody method.

Confirmation that the reflection modelling is correct has recently been obtained from X-ray reverberation [73]. This involves the small (tens of seconds to tens of minutes)
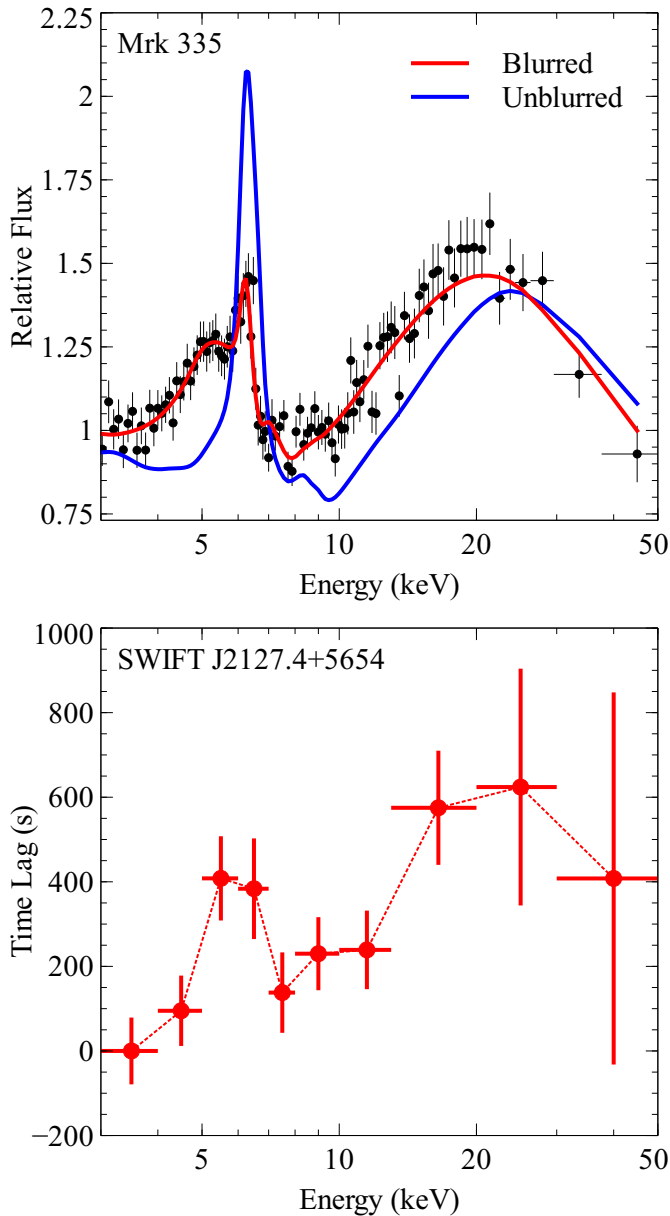
Figure 22. Upper: The unblurred reflection spectrum including the iron-K emission line and Compton hump (solid line) appears relativistically blurred to the observer as shown in the line fitted to the data points. The obvious dominant redshift is gravitational due to the proximity to the black hole. The source is the Seyfert galaxy Mkn335, observed by NuSTAR during a low state. Modelling of the data shows that the black hole in Mkn335 has a spin $a/M > 0.97$. Most of the emission seen in the spectrum emerges from within $2r_g$ of the event horizon [53]. Lower: Time lags measured by NuSTAR from the AGN SWIFTJ2127 showing both iron K and Compton peaks.

time delays or lags whch occur between the detection of an intrinsic change in luminosity of the corona and the corresponding change in the reflection. The energy spectrum of the high frequency time lags shows a broad iron line indicative of reflection (lower panel of Fig. 22).

The results for a number of objects imply that high spin is common for the brightest observed sources and the corona in those objects is compact and at a height of $5-10r_\mathrm{g}$. In this regime, strong light bending occurs such that much of the coronal emission is bent down to the disc making the reflection strong. Month-long temporary episodes have been seen in a few sources in which the continuum drops to being almost unobservable, with only slight changes to the reflected spectrum. It appears that the corona has dropped below $5r_\mathrm{g}$ in these cases and that light bending is preventing much of the continuum being observed at all. Most of the reflection spectrum is then emerging from within $2-3r_\mathrm{g}$, which is the closest emission easily seen from around any black hole [53].

Further evidence of a compact corona is obtained from microlensing studies of distant quasars which are lensed by intervening galaxies. This produces several images of the quasar which follow different light paths through the galaxy. Stars in the galaxy crossing one of those paths amplify the image by lensing to a degree depending on how the angular sizes of the emission region of the quasar and the Einstein ring of the star match one another. For typical values this means that higher amplitude variability is expected from smaller emission regions. Both optical and X-ray observations have been made of several lensed quasars which show that the X-ray emission region is much smaller than the optical one, and in several cases is less than $10r_\mathrm{g}$ in size [3].

10 Future Observations of Astrophysical Black Holes

Many exciting developments are expected over the next decade or so in observational studies of black holes. One important step will be the networking together of several millimetre-wavelength telescopes to form the Event Horizon Telescope which will resolve the "shadow" of the black hole in Sgr A* [13]. Extreme light bending of the emission from the accretion flow onto the black hole should reveal a dark patch, the shadow, at the position of the black hole. The diameter of the shadow is determined by the paths of light rays emitted from just above the event horizon to the observer and corresponds to about $10r_\mathrm{g}$ almost independent of the black hole spin.

Calculation of the shadow radius:
We use the results above for the photon effective potential in the Schwarzschild case. Putting together equations (9.3) and (9.4), we find

$$\frac{\dot{r}^2}{h^2} + \frac{1}{r^2}\left(1 - \frac{2\mu}{r}\right) = \frac{1}{b^2} \tag{10.1}$$

where $\mu = GM/c^2$ and b has been defined as h/kc. Note the dot here is not derivative w.r.t. proper time, which is zero for a photon, but w.r.t. an affine parameter along the path. We do not need to identify this parameter explicitly, since we are going to work with the shape *of the orbit. Specifically, noting $r^2\dot\phi = h$, we have*

$$\left(\frac{\dot r^2}{r^4\dot\phi^2}\right)^{1/2} = \frac{1}{r^2}\frac{dr}{d\phi} = \left(\frac{1}{b^2} - \frac{1}{r^2}\left(1 - \frac{2\mu}{r}\right)\right)^{1/2} \quad (10.2)$$

Solving (10.2) for $\mu = 0$, which is the limit where the only role of the central mass is to define the origin of the (r,ϕ) system), we get $r = b/\sin\phi$. This is the equation of a straight line, which if it continued all the way past the central object, would pass it with perpendicular distance b, so we can identify this b as the impact parameter. This generalises what we did above, where we considered the case of a light ray just grazing the surface of an object of radius R, for which the unperturbed solution was given by (9.5), i.e. $r = R/\sin\phi$.

Now we consider the exact equation again, and relate to a black hole. We know from the plot of photon effective potential in Fig. 18, that photons straying inside $r = 3GM/c^2$ are not free to escape to infinity. We therefore want to use this distance as the radius of an 'object' which the incoming photon just grazes. Using R for this object radius, we have

$$\left.\frac{dr}{d\phi}\right|_{r=R} = 0$$

This tells us that

$$\frac{1}{b^2} = \frac{1}{R^2}\left(1 - \frac{2\mu}{R}\right) \quad i.e. \quad b = R\left(\frac{R}{R - 2\mu}\right)^{1/2}$$

This expression is valid generally, and e.g. tells us that the Sun's effective shadow is about 3 km bigger than its coordinate radius, but applied with $R = 3GM/c^2$ for a black hole, we find $b = 3\sqrt 3 GM/c^2$, which is therefore the radius of the geometric shadow cast. Interestingly, the main effect of including black hole spin in the calculation is to cause a shift in the centroid of the shadow rather than its size — see e.g. [22] for details.

For Sgr A* this distance we have just worked out corresponds to an angular diameter of 52 microarcsec. This is 2.5×10^{-10} radians, and is very small indeed. Nevertheless, the angular resolution, approximately equal to the ratio of observing wavelength to telescope diameter, is about 20 microarcsec for intercontinental mm VLBI where the effective telescope diameter is 10,000 km.

Interestingly, the 6 billion $M_\odot$ black hole in M87 is 1500 times more massive than Sgr A* and 2000 times further away which makes its event horizon appear only slightly smaller, at 40 microarcsec. Plans are also underway to resolve the M87 black hole shadow, together with the base of its jet which should help us understand how it is

accelerated. All other black holes subtend smaller angular sizes. 3C273, for example, is 34 times more distant than M87, so its shadow will be about 1 microarcsec in size.

Near infrared interferometry at ESO's Very Large Telescope in Chile will use wavelengths around 2 microns and effective diameters of a 100 m to give a resolution of 4 milliarcsec. This will not resolve the black hole shadow but will resolve the motion of the orbiting stars much more precisely, particularly as the positional accuracy can be more than an order of magnitude better than the resolution. General relativistic effects on the orbits will be seen and fainter, possibly closer, stars resolved.

Of great interest would be a pulsar orbiting Sgr A*, which if a millisecond pulsar could prove to be a very stable and reliable orbiting clock. None have been found yet and the ionized plasma that bathes the inner region is a problem for sensitive radio searches. A type of pulsar called a magnetar was found in 2013 within 3 arsec of Sgr A*, but this magnetar unfortunately appears to be rather unreliable as a clock [10].

A gas cloud, G2, was discovered on a highly eccentric orbit close to Sgr A* in 2012 [56]. At pericentre in 2014, about 3 Earth masses of material passes within about $2000r_S$. Ram pressure from the accretion flow should cause it to spiral inward over the following few years leading to an increased accretion rate and associated display. It is in a similar path to an earlier discovered cloud G1 and other clouds. Their apocentre and orbital plane lie close to the orbits of some of the surrounding luminous stars. The winds of the stars may be the origin of the inspiralling gas clouds.

Further past activity of Sgr A* has been revealed by X-ray fluorescent emission lines seen from molecular clouds many tens to hundreds of light years out from the Galactic Centre. One interpretation suggests that the luminosity of Sgr A* may have been almost a million times higher about 100 yr ago [7].

Sufficient numbers of black hole spin measurements are expected from X-ray studies of AGN that the spin history can begin to be understood. Present work indicates many high spin objects in the mass range from $10^6 - 5 \times 10^7 M_\odot$. The accretion flow within $10r_g$ and particularly within $3r_g$ will be mapped and the corona understood. Indeed the whole power output of accreting black holes in terms of radiation, winds and jets will be explored.

Tidal disruption events due to stars straying close to a massive black hole are beginning to be observed. Black holes with masses above $10^8 M_\odot$ can swallow stars whole in the sense that they are not tidally disrupted until within the event horizon. The tidal forces of the more common lower-mass black holes can however destroy stars at greater distances leading to the production of a short lived, very luminous, accretion disc which decays with a timescale of about a year.

Studies of AGN feedback will accelerate with use of telescopes such as the Atacama Large Millimtre Array ALMA, the James Webb Space Telescope JWST, the Large Synoptic Survey Telescope LSST and the Advanced Telescope for High Energy Astronomy Athena. The growth of massive black holes through accretion and mergers will become understood.

Actually testing GR with black holes is difficult. The astrophysical phenomena

observed so far are explained within the Kerr metric. Some precision tests may occur if a pulsar is serendipitously found in a close orbit around a stellar mass black hole in our Galaxy or around Sgr A*. The discovery of gravitational waves from merging black holes will of course transform this aspect of the study of black holes.

More generally, the detection of gravitational waves emitted in events involving black holes has great potential for tying down aspects of astrophysical black holes that are poorly understood at present. These include the numbers of intermediate mass holes in the range between stellar mass black holes and SMBHs in galactic centres, and the evolution of the number density of black holes with cosmic epoch. Both these aspects are key targets for a future space-borne gravitational wave detector mission, such as eLISA or a future variant, and form a key component of its science mission [17]. There are many further aspects to the importance of gravitational waves in black hole astrophysics, but we defer coverage of these to other chapters of this book.

11 More general spherically symmetric black holes

Real black holes are embedded in a universe in which we know there are effects matching those of a cosmological constant, accounting for about 0.7 of the total energy density. Thus it is of interest to embed a black hole in a de Sitter universe. Additionally, black holes in anti-de Sitter universes are very interesting objects theoretically, since via the AdS/CFT correspondence (see e.g. [38]), the strong gravity effects of black holes can be replaced by weak perturbative effects in a conformal field theory living on the boundary of an anti-de Sitter space (though we note that the dimensionality involved does not necessarily match that of 4d spacetime).

Returning to the derivations of Section 2.1, we find that to satisfy the new field equation

$$G_{\mu\nu} + \Lambda g_{\mu\nu} = -8\pi T_{\mu\nu} \tag{11.1}$$

arising from introducing a cosmological constant Λ, the new equations the Ricci tensor has to satisfy are

$$R_{\mu\nu} = \Lambda g_{\mu\nu} \tag{11.2}$$

Using the components already given for the Ricci in (2.10) and above, one finds that this leads to a simple modification to the Schwarzschild values of A and B. We find that B is still equal to the inverse of A, and that now

$$A = 1 - \frac{2GM}{rc^2} - \frac{\Lambda}{3}r^2 \tag{11.3}$$

These are therefore the metric coefficients for a black hole of mass M embedded in a de Sitter universe, if Λ is positive, and anti-de Sitter, if Λ is negative.

Horizons occur (for our current form of the metric) when $B \to \infty$, hence here where $A = 0$. If $\Lambda > 0$, this now leads to an additional horizon being present, beyond

the Schwarzschild one near the black hole centre, at a position close to $r = \sqrt{3/\Lambda}$ (we are adopting a convention here in which Λ has dimensions length^{-2}). This is a version of the 'de Sitter horizon' — its exact position is modified slightly by the presence of the mass.

A further generalisation we can make, is to the case where the black hole is charged. As mentioned earlier, this is less compelling physically, since we do not expect significant charge separation to have occurred in the formation of a black hole, but the solution for this type of black hole, called the Reissner-Nordstrom solution (see e.g. [75] for references), is still of great interest theoretically. This also falls into our general scheme, and in fact the most general spherically symmetric black hole, which we can dub RNdS, for Reissner-Nordstrom-de Sitter, is given by

$$B = A^{-1}, \quad A = 1 - \frac{2GM}{rc^2} - \frac{\Lambda}{3}r^2 + \frac{q^2}{r^2} \tag{11.4}$$

where q is the black hole charge. Note there are now (in general) three *horizons. The Reissner-Nordstrom solution on its own introduces two horizons — one like the normal Schwarzschild one, and another usually much smaller one associated with the charge — and then for $\Lambda > 0$ there is an additional de Sitter horizon.*

An advantage of dealing with all these cases via the A, B form of the metric, is that we can give a unified treatment of energies and angular momenta in orbits. Repeating the analysis of Section 3 for this new case, we already have $\dot{r}$ from (3.8) and can get $\ddot{r}$ from

$$\frac{d}{dr}\left(\dot{r}^2\right) = \frac{d}{d\tau}\left(\dot{r}^2\right)\frac{d\tau}{dr} = \frac{2\ddot{r}\dot{r}}{\dot{r}} = 2\ddot{r}$$

For a circular orbit, both $\dot{r}$ and $\ddot{r}$ have to vanish and this combination of expressions therefore says that

$$-\frac{k^2}{A^2}A' + \frac{2h^2}{r^3} = 0$$

where $A' \equiv dA/dr$. Combining again with the expression for $\dot{r} = 0$ we can solve for k^2 and h^2, obtaining

$$k^2 = \frac{2A^2}{2A - rA'}, \quad and \quad h^2 = \frac{r^3 A'}{2A - rA'}$$

So we now have the energy and angular momentum for a particle in a circular orbit for quite a wide range of metrics. To calculate criteria for stability, one can show that it is useful to work in terms of the quantity (see Lasenby (2014) in preparation)

$$T(r) = \left(\frac{v}{c}\right)^2 = \tanh^2 u \tag{11.5}$$

where v is the velocity in a circular orbit at radius r and u is the corresponding rapidity parameter. From what we have already derived, one can show

$$T = \frac{rA'}{2A} \quad and \quad r\dot{\phi} = \gamma v = \sinh u \tag{11.6}$$

and then the criterion for stability turns out to be that

$$2T^2 - rT' - 2T \qquad (11.7)$$

should be negative. This simple criterion applies across all the spherically symmetric black hole cases. For example, inserting the A appropriate for a Schwarzschild-de Sitter metric, (11.3), we find the stability criterion

$$18M^2 - 15M\Lambda r^3 - 3Mr + 4\Lambda r^4 < 0 \qquad (11.8)$$

for stable circular orbits (in units with $c = G = 1$). For appropriate astrophysical values of M and Λ, and restoring units, the outer solution to this is well approximated by

$$r_{\text{stab}} \approx \left(\frac{3GM}{4\Lambda c^2} \right)^{1/3} \qquad (11.9)$$

We can apply this formula for any central mass, not just a black hole, and one can show that e.g. for a cluster of galaxies with $M = 10^{15} M_\odot$, and for the measured value of the cosmological constant, then $r_{\text{stab}} \approx 7.2 \, \text{Mpc}$. This is interestingly close to the maximum cluster sizes observed, though of course circular orbit stability is not likely to be the direct criterion one would apply in this case, where effects on velocity dispersion would be more appropriate (see [46] for further details).

12 Primordial black holes

Primordial black holes could have formed as a result of the high densities present soon after the Big Bang [8]. Their masses would be comparable to the particle horizon mass at their formation so it can range from the Planck mass (10^{-8} kg) at the Planck time (10^{-43} s), to $10^5 M_\odot$ at a time of 1 s. Primordial black holes of mass 10^{12} kg would have formed at 10^{-23} s and would be evaporating now due to the emission of Hawking radiation (see below), which would peak at 100s of MeV. Observations provide a limit on the background intensity of 100 MeV gamma-rays such that evaporating primordial black holes cannot account for more than 10^{-8} of the critical density of the Universe [52]. The frequency, energies and timescales of the final explosions do not match typical observed gamma-ray bursts. It is therefore unlikely that they are an important constituent of the Universe.

12.1 Hawking radiation

An initially very surprising result about black holes was proved by Hawking in 1974 [28]. This is that despite their name, the horizon radiates energy, as though it was a blackbody at the temperature of

$$T = \frac{\hbar c^3}{8\pi k_{\text{B}} GM} \qquad (12.1)$$

where k_B is the Boltzmann constant and M is the black hole's mass. The types of black hole we have mainly considered have a minimum mass of several $M_\odot$, and so their temperatures are less than $\sim 6 \times 10^{-8}$ K, and therefore negligibly tiny. However, a 10^{12} kg primordial black hole of the type mentioned above, would have a temperature of $\sim 1.2 \times 10^{11}$ K, and would therefore produce highly energetic radiation.

The emission process as calculated originally by Hawking was explained in terms of particle production in a second quantised treatment of a massless scalar field surrounding the black hole, but the principles extend to all kinds of field, massive or massless, which will be radiated with 'statistics' (i.e. Bose-Einstein or Fermi-Dirac) as appropriate to their spin, and with a thermal distribution with the temperature (12.1).

A heuristic way of demonstrating this effect is to consider vacuum fluctuations in the space just outside the horizon, which will lead to the production of virtual particle/antiparticle pairs there. Sufficiently close to the horizon, one of the pair will be able to 'tunnel' through the horizon and inside can become a real particle with negative energy. (The possibility of negative energy arises since as we saw above (Section 7.1), the timelike vector in the t-direction tips over to become spacelike inside the horizon, which coincides with the Stationary Limit surface in the Schwarzschild case, and so the projection of the particle momentum onto the local t-vector may be negative.) The particle remaining outside, which has positive energy, can therefore be emitted off to infinity, whilst the absorption of a negative energy particle by the black hole, decreases the mass M, thus providing the overall energy for the emission.

This type of derivation can be used to calculate the energy of the emitted particle, which turns out to be independent of exactly where (though assumed to be close to the horizon) the virtual pair is produced, and yields an energy $E = k_B T$ which is only a factor of 2π higher than the correct result from (12.1) — see Chapter 11 of [30] for details.

A further possibility for a calculation avoiding the full rigours of quantum field theory (QFT), is to work with a first-quantised field surrounding the black hole. For example, a detailed derivation for a massive Dirac field is given in Section 8 of [35]. This yields precisely the result (12.1) together with the correct Fermi-Dirac statistics for a spin-1/2 particle, and the calculation can be extended to electromagnetic and scalar particles, with the same results that would be obtained from QFT in each case (Lasenby et al *unpublished). However, it is only in a QFT context that one can be properly certain of the physics involved, and of how to go about making unique choices for the branches of analytic functions that are involved, and so a QFT approach is still necessary to be fully confident of the results.*

12.2 Link with surface gravity

What a full QFT approach leads to is a very general result that singles out the 'surface gravity' of a black hole (of any type) as the important quantity. The surface gravity

would appear to be infinite at the horizon, since no particle can escape the black hole's pull there. However, the definition of surface gravity intended here is that appropriate to the force felt at the horizon, but which would be evaluated by an observer at infinity. In e.g. [75], Exercise 6.4, this force is shown to differ from that at the horizon by the redshift factor from the horizon to infinity, which is also infinite. Specifically, one finds for a Schwarzschild black hole that the local force necessary to keep an observer of mass m stationary at radial distance r is (see e.g. Section 7 of [35])

$$F = \frac{GMm}{r^2} \left(1 - \frac{2GM}{rc^2}\right)^{-1/2} \qquad (12.2)$$

The gravitational redshift factor between the horizon and infinity is $\left(1 - \frac{2GM}{rc^2}\right)^{1/2}$, hence multiplying by this, we obtain the simple expression GMm/r^2 as the force that the observer at infinity would ascribe as being necessary to keep the observer at radius r at rest. (In the exercise in Wald ([75]), this difference is explained in terms of the different tensions necessary at the ends of a (massless) rope that extends from the observer at infinity to the one at radius r.)

This may seem a mundane and wholly Newtonian result, and exactly what we would expect 'at ininity'. However, we are now entitled to put $r = 2GM/c^2$, i.e. the value of r at the horizon, into this expression, in order to evaluate the 'surface gravity' of the black hole. This is defined as acceleration per unit mass, and customarily denoted κ, so we have found

$$\kappa = \frac{c^4}{4GM} \qquad (12.3)$$

The contribution of QFT at this point, is to tell us that a horizon with surface gravity κ radiates particles with a thermal temperature

$$T = \frac{\hbar\kappa}{2\pi k_{\mathrm{B}} c} \qquad (12.4)$$

Unruh in 1976 [71] showed that this is the temperature of a thermal heat bath that develops around an observer accelerating at rate κ in Minkowski space. We can now understand the link with surface gravity in black holes, at least heuristically. By the equivalence principle and working close to the horizon so that global curvature effects are not important, we can expect that the heat bath seen by a stationary observer feeling the effects of the black hole surface gravity κ, should be the same as the heat bath seen by an observer in Minkowski space accelerating at the same rate, and we can see indeed that equations (12.3) and (12.4) agree with (12.1) for this Schwarzschild case. The advantage of this route, however, is that if we work out the surface gravity in more complicated cases, such as for Kerr or Kerr-Newman or even de Sitter spacetimes (which as we have seen, also possess a horizon), then we can make the same transition to temperature as via (12.4). For example, for our general spherically symmetric

metric (2.7), it is easy to show that the surface gravity is

$$\kappa = \left.\frac{A'}{2\sqrt{AB}}\right|_{B^{-1}=0} \tag{12.5}$$

(The point where $1/B = 0$ is picked out as being the position of the event horizon.) Evaluating this for the Reissner-Nordstrom metric discussed above, and for clarity temporarily putting $G = c = 1$ etc., so $1/B = A = 1 - 2M/r + q^2/r^2$, we find that the surface gravity at the outer horizon is

$$\kappa_{RN} = \frac{\sqrt{M^2 - q^2}}{\left(M + \sqrt{M^2 - q^2}\right)^2} \tag{12.6}$$

and the Hawking temperature of the radiation emitted in this case is given by inserting this κ into (12.4).

12.3 Astrophysical aspects of black hole evaporation

We can compute the rate at which a Schwarzschild black hole loses mass via the formula for the luminosity of a blackbody at temperature T, i.e. σT^4 where $\sigma = \pi^2 k_{\mathrm{B}}^4/(60\hbar^3 c^2)$ is the Stefan-Boltzmann constant, together with the area of the horizon, which is $4\pi(2GM/c^2)^2$. This yields

$$\dot{M}c^2 = -power\ radiated = -\frac{c^6\hbar}{15360\,\pi G^2 M^2} \tag{12.7}$$

Solving this differential equation, we find that the cube of the mass declines linearly with time:

$$M^3(t) = M_0^3 - \frac{c^4\hbar}{5120\,\pi G^2}t \tag{12.8}$$

where M_0 is the initial mass and t is measured from formation. This gives an evaporation time in terms of M_0 of

$$t_{\mathrm{evap}} = 2.66 \times 10^{-24} M_0^3 \text{ yrs} \tag{12.9}$$

If the current age of the universe is 13.8 billion years, this means only black holes with a mass less than 1.7×10^{11} kg will have had a chance to decay by now. Due to the M^{-2} dependence in the expression for radiated power, (12.7), nearly all the energy emitted is confined to the very last moments of the black hole's life.

12.4 Black hole entropy

The fact that black holes radiate like black bodies, suggest that they should have an entropy. If we identify Mc^2 as the hole's energy, then the thermodynamic relation

$$dU = TdS \tag{12.10}$$

along with our identification of the BH temperature in (12.1), yields (first working in units with $G = \hbar = c = k_B = 1$ for clarity)

$$dM \times 8\pi M = dS, \quad so \ that \quad S = 4\pi M^2 = \frac{\mathcal{A}}{4} \tag{12.11}$$

where $\mathcal{A} = 16\pi M^2$ is the black hole area. Putting back the units, we find that the black hole entropy in units of k_B, is

$$\frac{S}{k_B} = \frac{\mathcal{A}}{4\ell_p^2} \tag{12.12}$$

where $\ell_P = \sqrt{\hbar G/c^3}$ is the Planck length and $\mathcal{A} = 4\pi(2GM/c^2)^2$ is the BH area. For an astrophysical black hole, this entropy is large, and as we have seen scales like M^2. The result of this is that it is thought that supermassive black holes in the centres of galaxies dominate the entropy budget of the observable universe. Estimates of this are given in [15], with the result that SMBH may contribute up to 7 orders of magnitude more entropy than stellar mass BHs, and approximately 15 orders of magnitude more than the next largest component, due to photons.

This identification of entropy with 1/4 of the event horizon area expressed in units of ℓ_p^2, is the starting point for a great deal of work connected with whether a microphysics approach to black hole entropy is possible. In this approach we would seek to obtain the same result by counting states, and then assigning $S = k_B \ln N$, where N is the number of available microstates. A related question is what happens to the information about the matter and radiation from which the hole was originally formed. This information is screened beyond the horizon, and our lack of knowledge of the internal arrangements and compositions of this original material provides a satisfactory understanding of why the black hole should have an entropy at all, as already proposed by Beckenstein [2], before *Hawking's discovery of black hole radiation. However, at the end stage of evaporation of the black hole, we no longer have a screen, and unless the information is somehow encoded in the phases of the emitted particles and fields composing the Hawking radiation, so that this is not random after all, then the information has been irretrievably lost. This would seem to violate the basic principles of quantum mechanics, which demand* unitarity *of transformations between beginning and end states, and would not allow the disappearance of information in this way, given that there is no longer a casual horizon beyond which the information is hidden.*

These are deep and fundamental questions, which we do not venture further with, but are discussed elsewhere in this volume. We note that our discussion so far has been just in terms of a Schwarzschild black hole, but equivalences of the same nature work for all types of black hole, and are encoded in the 'Laws of black hole thermodynamics'. We now briefly discuss these concentrating on their astrophysical implications, and in particular the possibility of extracting energy from rotating black holes.

12.5   Laws of black hole thermodynamics and the Penrose process

The generalisation of (12.10) to an uncharged rotating black hole reads (in natural units again, for clarity):

$$dU = T dS + \Omega_H dJ$$
$$i.e. \quad dM = \frac{\kappa}{8\pi} d\mathcal{A} + \Omega_H dJ$$

$$(12.13)$$

where Ω_H is the black hole angular velocity at the horizon, and we have again made the identification of temperature with surface gravity/2π and of entropy with one quarter of the horizon area. The new feature here is that work can be done to change the angular momentum J of the black hole. (Recall that this is related to the mass and spin parameters via $J = aM$.)

Equation (12.13) is known as the 'First law of black hole thermodynamics'. There are equivalent versions for black holes of the other three laws of thermodynamics as well — see e.g. Section 9.9 of [22] for a discussion of these. For astrophysical processes, the other law of immediate interest is the equivalent of the Second law, which states that in any classical process, the area of a black hole horizon, which we know measures the black hole's entropy, does not decrease. The restriction to classical processes is necessary, since as we have seen, Hawking radiation succeeds in reducing both mass and surface area.

The most interesting immediate application of these laws is to (classical) processes in which we attempt to remove energy from the hole. This cannot be done for a non-rotating hole, but the $\Omega_H dJ$ term in the First law provides a route through to this for rotating holes.

The first process of this kind to be discussed, was the Penrose process [54]. In this process, an incoming particle enters the ergosphere of the black hole. It then decays into two particles. Particles can escape from the ergosphere (which lies outside the horizon), and we arrange the initial trajectory and decay such that one of the decay products escapes, and the other falls into the black hole. The key observation is now that inside the ergosphere the g_t Killing vector corresponding to invariance of the metric under time displacements, becomes spacelike, (remember the definition of the ergosphere is where g_t^2 changes sign), and it is possible for a particle to have negative energy when its 4-momentum is projected onto it. If this happens, then from conservation of energy, the energy of the emitted particle will be greater than that of the original particle, and we will have succeeded in extracting energy from the black hole. This energy has come via the BH's absorption of the infalling negative energy particle.

One can also analyse what happens to angular momentum in this process, by considering the projections onto the other Killing vector (corresponding to ϕ invariance of the metric) g_ϕ. This reveals (see [77] or [22] for details) that the hole absorbs negative angular momentum as well as negative energy (meaning the emitted particle

enjoys a boost to its angular momentum as well as energy, relative to the incoming one) and that the black hole parameter changes obey the inequality

$$\delta M \geq \Omega_H \delta J \tag{12.14}$$

Now, the expressions in the Kerr case for the quantities appearing in the First law (12.13) are

$$\text{Horizon area} \quad \mathcal{A} = 8\pi \left(M^2 + \sqrt{M^4 - J^2} \right)$$

$$\text{Horizon angular velocity} \quad \Omega_H = \frac{J}{2M \left(M^2 + \sqrt{M^4 - J^2} \right)} \tag{12.15}$$

$$\text{Surface gravity} \quad \kappa = \frac{\sqrt{M^4 - J^2}}{2M \left(M^2 + \sqrt{M^4 - J^2} \right)}$$

(again see [77] or [22] for details). We thus have that the response of the horizon area to a general change in M and J is

$$\delta \mathcal{A} = \frac{\partial \mathcal{A}}{\partial M} \delta M + \frac{\partial \mathcal{A}}{\partial J} \delta J = \frac{8\pi J}{\Omega_H \sqrt{M^4 - J^2}} \left(\delta M - \Omega_H \delta J \right) \tag{12.16}$$

From (12.14), we see that despite the fact that both M and J decrease, the r.h.s. here is always *positive in the Penrose process. This is an example of the Second law of black hole thermodynamics in action — for a classical process, the BH entropy, as measured by the horizon area, must always increase.*

12.6 Adiabatic (reversible) changes

An interesting case to consider astrophysically, is the limit of gradual changes in mass and angular momentum, which satisfy the thermodynamic notion of adiabaticity, *in particular the changes are reversible. This is possible, for example, for particular versions of the Penrose process. In the black hole context, since horizon area equates to entropy, an adiabatic process will have $\delta \mathcal{A} = 0$.*

Solving (12.16) for $\delta \mathcal{A} = 0$, immediately yields the following differential equation for $M(J)$:

$$\frac{dM}{dJ} = \Omega_H = \frac{J}{2M \left(M^2 + \sqrt{M^4 - J^2} \right)} \tag{12.17}$$

for which the following (implicit) solution works:

$$2M_0^2 = M^2(J) + \sqrt{M^4(J) - J^2} \tag{12.18}$$

where M_0 is a constant. As an example, suppose we start with a Schwarzschild black hole with mass M_0, and gradually feed in material with positive angular momentum.

We will be able to do this until an extremal black hole with $J = M^2$ is reached, at which point the mass is $\sqrt{2}M_0$. An interesting point is what happens to the horizon radius r_{outer} in this process. We know the general expression for it (in terms of M and $J = aM$) is

$$r_{\text{outer}} = M + \frac{1}{\sqrt{M}}\left(M^2 + \sqrt{M^4 - J^2}\right) \tag{12.19}$$

and naively we might expect this to increase as the hole gains mass. But in fact we can see for the adiabatic process just discussed,

$$r_{\text{outer}} = \frac{\mathcal{A}}{8\pi M} = \frac{16\pi M_0^2}{8\pi M} = \frac{2M_0^2}{M} \tag{12.20}$$

The horizon radius therefore goes down, *reaching a minimum of $\sqrt{2}M_0$ at the end of the process (corresponding to the $r_{\text{outer}} = M$ value for an extremal black hole), having started at $2M_0$.*

12.7 Other processes for extracting energy from a spinning black hole

As well as the Penrose process, there are other ways of extracting energy from a rotating black hole. One of these is 'superradiance', which is the analogue for waves of what happens for particles in the Penrose process. The possibility of such a process was first drawn attention to specifically in the context of the Kerr solution by Starobinski in 1973 [68]. It involves an incoming radiation field of the form

$$\phi \sim \phi_0(r,\theta)e^{-i\omega t}e^{m\phi} \tag{12.21}$$

for which part of the wave (the 'transmitted' wave) is absorbed by the black hole, and the other part (the 'reflected' wave) reaches infinity again. In the same way as for the Penrose process, due to the spacelike nature of the g_t Killing vector inside the ergosphere, the transmitted wave can have negative energy, so that the reflected wave carries increased energy to infinity (specifically it will have greater amplitude at the same frequency as compared to the incident wave). We can derive the condition for this to occur (at least in a heuristic way), as follows (see e.g. Section 8.8 of [22]).

We can think of the wave as composed of quanta with energy $\hbar\omega$ and angular momentum $\hbar m$. When these are absorbed by the black hole, the change in the black hole's parameters will satisfy

$$\frac{\delta J}{\delta M} = \frac{\hbar m}{\hbar \omega} \tag{12.22}$$

But we also know that $\delta M - \Omega_H \delta J \geq 0$ from the fact the horizon area must not decrease. Putting these together leads to

$$\frac{\delta M}{\omega}\left(\omega - \Omega_H m\right) \geq 0 \tag{12.23}$$

and so the condition for superradiance ($\delta M < 0$) is

$$0 < \omega < m\Omega_H \tag{12.24}$$

Further details of this process, which only works for bosonic fields, can be found in Section 12.4 of [75].

Our final example, concerns what may be an important way in which spinning black holes return energy to the environment, and which was referred to briefly above in Section 6.1, namely the Blandford-Znajek effect [4].

Here, one considers a Kerr black hole immersed in an ambient magnetic field, typically associated with an accretion disc around the black hole. A possible picture of the process (see e.g. [22] Section 8.9) represents the black hole horizon as a moving conductor within the magnetic field. Indeed the Kerr black hole horizon, in common with all stationary event horizons, can be modelled as having a resistance of 4π in geometrical units (377 Ohms in ordinary units). This rotating conductor coupled to the magnetic field, generates a current which flows between the poles and equator — it is in this sense like a dynamo. The main analytic field configuration chosen by Blandford & Znajek was a 'split monopole' — i.e. a different sign magnetic monopole solution in each hemisphere, with magnetic field lines pointing radially outwards or inwards. This needs a current sheet on the join between them in the equitorial plane, which is presumed to be supplied at least outside the hole by currents in the accretion disc.

The radiated power can be calculated from the Poynting vector, and gives similar results as for a rotating magnetic dipole pulsar model evaluated on the light cylinder. Specifically we find (see e.g. [40] Section 14.3)

$$
\begin{aligned}
\mathcal{P}^{\mathcal{EM}} &= \frac{B_E^2 r_E^4 \Omega_f^2}{c} = \frac{B_H^2 r_H^4 \Omega_f^2}{c} \\
&\sim 4.1 \times 10^{47} \text{ erg s}^{-1} \left(\frac{B_H}{10^5 \text{ G}}\right)^2 \left(\frac{a}{M}\right)^2 \left(\frac{M}{10^9 M_\odot}\right)^2
\end{aligned} \tag{12.25}
$$

Here B_E and B_H are the magnetic field values at the ergosphere and horizon respectively, r_E and r_H the corresponding r values, and Ω_f the magnetic field rotation rate, which is typically $\sim \frac{1}{2}\Omega_H$. This EM power will presumably be manifested in a magnetised particle wind and jet, removing angular momentum and energy from the black hole in the process. Subsequent work (see e.g. Komissarov [34]) has shown that the Blandford-Znajek (BZ) mechanism is stable, and clarified that important components of it take place within the ergosphere itself, emphasising its links with the Penrose process and superradiance. The BZ mechanism is now thought to be an important component in generating at least some of the high energy jets we see in astrophysics [69].

13 Conclusions

Black holes are now an integral features of our cosmic landscape. Many millions of stellar mass black holes reside in our Galaxy. A supermassive black hole lies at the centre of all massive galaxies. We know little about most of them, unless they are massive and nearby or accreting gas from a stellar companion or the surrounding interstellar medium. The inner part of the accretion flow can be extremely luminous. making the immediate surroundings of the blackest parts of the Universe into the brightest.

The behaviour of observed black holes can so far be explained well by General Relativity and the Kerr metric. The physics of accretion onto black holes, and of the outflows and jets that often accompany inflows, is complex and leads to complicated observational phenomena which lie at the forefront of astrophysics. Understanding how quasars work remains a significant astrophysical challenge. The consequences for a galaxy hosting a supermassive black hole are profound. It is likely that the energy released by the growth of the black hole plays a decisive factor in its final stellar mass and possibly its physical size.

Black holes are intrinsically relativistic objects which have stimulated and tested physical understanding to the extreme. The internal structure of the black hole, within the event horizon, is beyond direct observation and we have not discussed it here, although it is clearly of great theoretical interest. In this Chapter we have looked at black holes as observable physical objects and considered how they work as engines of gravitational energy release.

The future of research into astrophysical black holes is very bright, as more telescopes probe ever deeper into more wavebands to uncover new objects, features and phenomena. Serendipitous discovery plays a key role in the history of astronomy and we look forward to the discoveries of a millisecond pulsar orbiting close to a massive black hole, a rogues gallery of black hole shadows, a range of quasars above redshift 10, a complete X-ray spectral-timing deconstruction of the innermost accretion flow around a rapidly spinning black hole and, most of all, some new phenomena of black holes that we have not yet anticipated.

Bibliography

[1] S. Antoci and D.-E. Liebscher, Editor's Note: On the Gravitational Field of a Mass Point According to Einstein's Theory by K. Schwarzschild, *General Relativity and Gravitation* 35 (2003), 945–950.

[2] J.D. Bekenstein, Black holes and the second law, *Lett.Nuovo Cim.* 4 (1972), 737–740.

[3] J. A. Blackburne, C. S. Kochanek, B. Chen, X. Dai and G. Chartas, The Optical, Ultraviolet, and X-Ray Structure of the Quasar HE 0435-1223, ApJ 789 (2014), 125.

[4] R.D. Blandford and R.L. Znajek, Electromagnetic extraction of energy from Kerr black holes, *Mon.Not.Roy.Astron.Soc.* 179 (1977), 433–456.

[5] C. T. Bolton, Identification of Cygnus X-1 with HDE 226868, Nature 235 (1972), 271–273.

[6] Robert H. Boyer and Richard W. Lindquist, Maximal analytic extension of the Kerr metric, *J.Math.Phys.* 8 (1967), 265.

[7] R. Capelli, R. S. Warwick, D. Porquet, S. Gillessen and P. Predehl, The X-ray lightcurve of Sagittarius A* over the past 150 years inferred from Fe-Kα line reverberation in Galactic centre molecular clouds, A&A 545 (2012), A35.

[8] B. J. Carr, K. Kohri, Y. Sendouda and J. Yokoyama, New cosmological constraints on primordial black holes, Phys. Rev. D 81 (2010), 104019.

[9] S. Chandrasekhar, The Maximum Mass of Ideal White Dwarfs, ApJ 74 (1931), 81.

[10] J. Chennamangalam and D. R. Lorimer, The Galactic Centre pulsar population, MNRAS 440 (2014), L86–L90.

[11] E. Churazov, R. Sunyaev, W. Forman and H. Böhringer, Cooling flows as a calorimeter of active galactic nucleus mechanical power, MNRAS 332 (2002), 729–734.

[12] H. D. Curtis, Descriptions of 762 Nebulae and Clusters Photographed with the Crossley Reflector, *Publications of Lick Observatory* 13 (1918), 9–42.

[13] S. Doeleman, E. Agol, D. Backer, F. Baganoff, G. C. Bower, A. Broderick, A. Fabian, V. Fish, C. Gammie, P. Ho, M. Honman, T. Krichbaum, A. Loeb, D. Marrone, M. Reid, A. Rogers, I. Shapiro, P. Strittmatter, R. Tilanus, J. Weintroub, A. Whitney, M. Wright and L. Ziurys, Imaging an Event Horizon: submm-VLBI of a Super Massive Black Hole, in: *astro2010: The Astronomy and Astrophysics Decadal Survey*, Astronomy 2010, p. 68, 2009.

[14] C. Doran and A.N. Lasenby, New techniques for analyzing axisymmetric gravitational systems. 1. Vacuum fields, *Class.Quant.Grav.* 20 (2003), 1077–1102.

[15] C. A. Egan and C. H. Lineweaver, A Larger Estimate of the Entropy of the Universe, ApJ 710 (2010), 1825–1834.

[16] F. Eisenhauer, R. Genzel, T. Alexander, R. Abuter, T. Paumard, T. Ott, A. Gilbert, S. Gillessen, M. Horrobin, S. Trippe, H. Bonnet, C. Dumas, N. Hubin, A. Kaufer, M. Kissler-Patig, G. Monnet, S. Ströbele, T. Szeifert, A. Eckart, R. Schödel and S. Zucker, SINFONI in the Galactic Center: Young Stars and Infrared Flares in the Central Light-Month, ApJ 628 (2005), 246–259.

[17] The eLISA Consortium, The Gravitational Universe, *ArXiv e-prints 1305.5720* (2013).

[18] A. C. Fabian, The obscured growth of massive black holes, MNRAS 308 (1999), L39–L43.

[19] _____ , Observational Evidence of Active Galactic Nuclei Feedback, ARA&A 50 (2012), 455–489.

[20] A. C. Fabian, E. Kara and M. L. Parker, Relativistic Disc lines, *ArXiv e-prints* (2014).

[21] A. C. Fabian, M. J. Rees, L. Stella and N. E. White, X-ray fluorescence from the inner disc in Cygnus X-1, MNRAS 238 (1989), 729–736.

[22] Valeri P. Frolov and Andrei Zelnikov, *Introduction to black hole physics*, Oxford University Press, 2011.

[23] R. Genzel, F. Eisenhauer and S. Gillessen, The Galactic Center massive black hole and nuclear star cluster, *Reviews of Modern Physics* 82 (2010), 3121–3195.

[24] A. M. Ghez, M. Morris, E. E. Becklin, A. Tanner and T. Kremenek, The accelerations of stars orbiting the Milky Way's central black hole, Nature 407 (2000), 349–351.

[25] R. Giacconi, H. Gursky, F. R. Paolini and B. B. Rossi, Evidence for x Rays From Sources Outside the Solar System, *Physical Review Letters* 9 (1962), 439–443.

[26] S. Gillessen, F. Eisenhauer, T. K. Fritz, H. Bartko, K. Dodds-Eden, O. Pfuhl, T. Ott and R. Genzel, The Orbit of the Star S2 Around SGR A* from Very Large Telescope and Keck Data, ApJ 707 (2009), L114–L117.

[27] K. Gültekin, D. O. Richstone, K. Gebhardt, T. R. Lauer, S. Tremaine, M. C. Aller, R. Bender, A. Dressler, S. M. Faber, A. V. Filippenko, R. Green, L. C. Ho, J. Kormendy, J. Magorrian, J. Pinkney and C. Siopis, The M-σ and M-L Relations in Galactic Bulges, and Determinations of Their Intrinsic Scatter, ApJ 698 (2009), 198–221.

[28] S.W. Hawking, Black hole explosions, *Nature* 248 (1974), 30–31.

[29] C. Hazard, M. B. Mackey and A. J. Shimmins, Investigation of the Radio Source 3C 273 By The Method of Lunar Occultations, Nature 197 (1963), 1037–1039.

[30] M. P. Hobson, G. P. Efstathiou and A. N. Lasenby, *General Relativity: An Introduction for Physicists*, Cambridge University Press, 2006.

[31] Roy P. Kerr, Gravitational field of a spinning mass as an example of algebraically special metrics, *Phys.Rev.Lett.* 11 (1963), 237–238.

[32] A. King, The AGN-Starburst Connection, Galactic Superwinds, and M_{BH}-σ, ApJ 635 (2005), L121–L123.

[33] R. W. Klebesadel, I. B. Strong and R. A. Olson, Observations of Gamma-Ray Bursts of Cosmic Origin, ApJ 182 (1973), L85.

[34] S. S. Komissarov, Electrodynamics of black hole magnetospheres, MNRAS 350 (2004), 427–448.

[35] A. Lasenby, C. Doran and S. Gull, Gravity, gauge theories and geometric algebra, *Royal Society of London Philosophical Transactions Series A* 356 (1998), 487.

[36] D. Lynden-Bell, Galactic Nuclei as Collapsed Old Quasars, Nature 223 (1969), 690–694.

[37] J. Magorrian, S. Tremaine, D. Richstone, R. Bender, G. Bower, A. Dressler, S. M. Faber, K. Gebhardt, R. Green, C. Grillmair, J. Kormendy and T. Lauer, The Demography of Massive Dark Objects in Galaxy Centers, AJ 115 (1998), 2285–2305.

[38] Juan Martin Maldacena, The Large N limit of superconformal field theories and supergravity, *Int.J.Theor.Phys.* 38 (1999), 1113–1133.

[39] J. E. McClintock, R. Narayan, S. W. Davis, L. Gou, A. Kulkarni, J. A. Orosz, R. F. Penna, R. A. Remillard and J. F. Steiner, Measuring the spins of accreting black holes, *Classical and Quantum Gravity* 28 (2011), 114009.

[40] David L Meier, *Black Hole Astrophysics: The Engine Paradigm*, Springer, 2009.

[41] J. Michell, On the Means of Discovering the Distance, Magnitude, &c. of the Fixed Stars, in Consequence of the Diminution of the Velocity of Their Light, in Case Such a Diminution Should be Found to Take Place in any of Them, and Such Other Data Should be Procured from Observations, as Would be Farther Necessary for That Purpose. By the Rev. John Michell, B. D. F. R. S. In a Letter to Henry Cavendish, Esq. F. R. S. and A. S., *Royal Society of London Philosophical Transactions Series I* 74 (1784), 35–57.

[42] J. M. Miller, Relativistic X-Ray Lines from the Inner Accretion Disks Around Black Holes, ARA&A 45 (2007), 441–479.

[43] G. Miniutti, A. C. Fabian, R. Goyder and A. N. Lasenby, The lack of variability of the iron line in MCG-6-30-15: general relativistic effects, MNRAS 344 (2003), L22–L26.

[44] M. R. Morris, L. Meyer and A. M. Ghez, Galactic center research: manifestations of the central black hole, *Research in Astronomy and Astrophysics* 12 (2012), 995–1020.

[45] N. Murray, E. Quataert and T. A. Thompson, On the Maximum Luminosity of Galaxies and Their Central Black Holes: Feedback from Momentum-driven Winds, ApJ 618 (2005), 569–585.

[46] R. Nandra, A. N. Lasenby and M. P. Hobson, The effect of an expanding universe on massive objects, MNRAS 422 (2012), 2945–2959.

[47] R. Narayan and J. E. McClintock, Advection-dominated accretion and the black hole event horizon, *New.Astron.Rev.* 51 (2008), 733–751.

[48] E T. Newman, R. Couch, K. Chinnapared, A. Exton, A. Prakash and R. Torrence, Metric of a Rotating, Charged Mass, *J.Math.Phys.* 6 (1965), 918–919.

[49] I. D. Novikov and K. S. Thorne, Astrophysics of black holes., in: *Black Holes (Les Astres Occlus)* (C. Dewitt and B. S. Dewitt, eds.), pp. 343–450, 1973.

[50] J. R. Oppenheimer and H. Snyder, On Continued Gravitational Contraction, *Physical Review* 56 (1939), 455–459.

[51] J. A. Orosz, J. E. McClintock, R. Narayan, C. D. Bailyn, J. D. Hartman, L. Macri, J. Liu, W. Pietsch, R. A. Remillard, A. Shporer and T. Mazeh, A 15.65-solar-mass black hole in an eclipsing binary in the nearby spiral galaxy M 33, Nature 449 (2007), 872–875.

[52] D. N. Page and S. W. Hawking, Gamma rays from primordial black holes, ApJ 206 (1976), 1–7.

[53] M. L. Parker, D. R. Wilkins, A. C. Fabian, D. Grupe, T. Dauser, G. Matt, F. A. Harrison, L. Brenneman, S. E. Boggs, F. E. Christensen, W. W. Craig, L. C. Gallo, C. J. Hailey, E. Kara, S. Komossa, A. Marinucci, J. M. Miller, G. Risaliti, D. Stern, D. J. Walton and W. W. Zhang, The NuSTAR spectrum of Mrk 335: extreme relativistic effects within two gravitational radii of the event horizon?, MNRAS 443 (2014), 1723–1732.

[54] R. Penrose, Gravitational Collapse: the Role of General Relativity, *Nuovo Cimento Rivista Serie* 1 (1969), 252.

[55] B. M. Peterson, Measuring the Masses of Supermassive Black Holes, Space Sci. Rev. (2013).

[56] O. Pfuhl, S. Gillessen, F. Eisenhauer, R. Genzel, P. M. Plewa, T. Ott, A. Ballone, M. Schartmann, A. Burkert, T. K. Fritz, R. Sari, E. Steinberg and A.-M. Madigan, The Galactic Center cloud G2 and its gas streamer, *ArXiv e-prints 1407.4354* (2014).

[57] T. Piran, The physics of gamma-ray bursts, *Reviews of Modern Physics* 76 (2004), 1143–1210.

[58] J. E. Pringle, M. J. Rees and A. G. Pacholczyk, Accretion onto Massive Black Holes, A&A 29 (1973), 179.

[59] R. A. Remillard and J. E. McClintock, X-Ray Properties of Black-Hole Binaries, ARA&A 44 (2006), 49–92.

[60] E. E. Salpeter, Accretion of Interstellar Matter by Massive Objects., ApJ 140 (1964), 796–800.

[61] M. Schmidt, 3C 273 : A Star-Like Object with Large Red-Shift, Nature 197 (1963), 1040.

[62] E. L. Schucking, The first Texas symposium on relativistic astrophysics, *Physics Today* 42 (1989), 46–52.

[63] K. Schwarzschild, On the Gravitational Field of a Mass Point According to Einstein's Theory, *General Relativity and Gravitation* 35 (2003), 951–959.

[64] C. K. Seyfert, Nuclear Emission in Spiral Nebulae., ApJ 97 (1943), 28.

[65] N. I. Shakura and R. A. Sunyaev, Black holes in binary systems. Observational appearance., A&A 24 (1973), 337–355.

[66] J. Silk and M. J. Rees, Quasars and galaxy formation, A&A 331 (1998), L1–L4.

[67] A. Soltan, Masses of quasars, MNRAS 200 (1982), 115–122.

[68] A. A. Starobinskiǐ, Amplification of waves during reflection from a rotating "black hole", *Soviet Journal of Experimental and Theoretical Physics* 37 (1973), 28.

[69] A. Tchekhovskoy, R. Narayan and J. C. McKinney, Efficient generation of jets from magnetically arrested accretion on a rapidly spinning black hole, MNRAS 418 (2011), L79–L83.

[70] K. S. Thorne, Disk-Accretion onto a Black Hole. II. Evolution of the Hole, ApJ 191 (1974), 507–520.

[71] W.G. Unruh, Notes on black hole evaporation, *Phys.Rev.* D14 (1976), 870.

[72] C. M. Urry and P. Padovani, Unified Schemes for Radio-Loud Active Galactic Nuclei, PASP 107 (1995), 803.

[73] P. Uttley, E. M. Cackett, A. C. Fabian, E. Kara and D. R. Wilkins, X-ray reverberation around accreting black holes, *ArXiv e-prints* (2014).

[74] M. van der Klis, Millisecond Oscillations in X-ray Binaries, ARA&A 38 (2000), 717–760.

[75] Robert M. Wald, *General Relativity*, University of Chicago Press, 1984.

[76] B. L. Webster and P. Murdin, Cygnus X-1-a Spectroscopic Binary with a Heavy Com-
      panion?, Nature 235 (1972), 37–38.

[77] A. Zee, *Einstein gravity in a nutshell*, Princeton University Press, 2013.

[78] Y. B. Zel'dovich, The Fate of a Star and the Evolution of Gravitational Energy Upon
      Accretion, *Soviet Physics Doklady* 9 (1964), 195.

Author information

Andrew C. Fabian, Institute of Astronomy, Madingley Road, Cambridge, CB3 0HA, UK.
E-mail: `acf@ast.cam.ac.uk`

Anthony N. Lasenby, Kavli Institute for Cosmology, Madingley Road, Cambridge, CB3 0HA
and Cavendish Laboratory, J. J. Thomson Avenue, Cambridge, CB3 0HE, UK.
E-mail: `a.n.lasenby@mrao.cam.ac.uk`